Asymmetric synthesis of enantiopure tetracyclic dispirooxindolopyrrolidine-piperidones via microwave-assisted multicomponent reaction: crystallographic analysis, antimicrobial activity and in silico studies

Hanen Jelizi, Amani Toumi, Faiza I.A. Abdella, Ismail Daoud, Sarra Boudriga, Asma Alshamari, Tahani Y.A. Alanazi, Ahlam Abdulrahman Alrashdi, Hayet Edziri, Michael Knorr, et al.

Journal of Molecular Structure 1308 (2024) 138104

Contents lists available at ScienceDirect

Journal of Molecular Structure

journal homepage: www.elsevier.com/locate/molstr

Asymmetric synthesis of enantiopure tetracyclic dispirooxindolopyrrolidine-piperidones *via* microwave-assisted multicomponent reaction: Crystallographic analysis, antimicrobial activity and *in silico* studies

Hanen Jelizi [a], Amani Toumi [a], Faiza I.A. Abdella [b], Ismail Daoud [c,d], Sarra Boudriga [a,*], Asma K. Alshamari [b], Tahani Y.A. Alanazi [b], Ahlam Abdulrahman Alrashdi [b], Hayet Edziri [e], Michael Knorr [f,*], Jan-Lukas Kirchhoff [g], Carsten Strohmann [g]

[a] *Laboratory of Heterocyclic Chemistry Natural Product and Reactivity (LR11ES39), Department of Chemistry, Faculty of Science of Monastir, University of Monastir, Monastir 5019, Tunisia*
[b] *Department of Chemistry, College of Science, Ha'il University, Ha'il 81451, Saudi Arabia*
[c] *Department of Matter Sciences, University of Mohamed Khider, BP 145 RP, Biskra 07000, Algeria*
[d] *Laboratory of Natural and Bio-Actives Substances, Faculty of Science, Tlemcen University, P.O. Box 119, Tlemcen 13000, Algeria*
[e] *Laboratoire des Maladies Transmissibles et des Substances Biologiquement Actives, Faculté de Pharmacie, Monastir 5000, Tunisia*
[f] *Université de Franche-Comté, Institut UTINAM-UMR CNRS 6213, 16 Route de Gray, Besançon 25030, France*
[g] *Faculty of Chemistry, Inorganic Chemistry, Technical University Dortmund, Otto-Hahn-Strasse 6, Dortmund 44227, Germany*

ARTICLE INFO

Keywords:
Microwave-assisted synthesis
Multicomponent reaction
1,3-dipolar cycloaddition
Spirooxindole
Piperidone
SC-XRD analysis
Antimicrobial activity
Molecular docking studies

ABSTRACT

In an attempt towards the development of new antimicrobials, we synthesized by microwave-assisted multicomponent reaction (MCR) of enantiopure *(E,E)*-3,5-bisarylidene-*N*-[(*S*)-(-)-methylbenzyl]-4-piperidones, isatin and α-amino esters a series of optically active tetracyclic dispirooxindolopyrrolidine-piperidones. The beneficial and promising features of this protocol such as simple operational procedure, short reaction time (10 min), and high product yields (up to 97 %) make it an efficient eco-friendly approach offering a powerful mean to expand the structural diversity of spirooxindoles. This approach appears hugely advantageous for high-throughput screening processes in drug discovery research. In addition, crystallographic parameters and inter- and intramolecular interactions occurring in spiropyrrolidine-fused piperidone derivative **4g** were examined through single-crystal XRD analysis allowing to determine the absolute configuration of the enantiopure compound. The preliminary biological assessment of their antimicrobial activity indicates that most of the screened products display higher activity than the standard reference drugs Ampicillin and Griseofulvin. Some of them exhibited good to moderate activity against both bacteria and fungi. In addition, *in silico* molecular docking and predictive ADMET studies for the most active spirocompounds were carried out. Molecular docking confirmed the binding efficacy of candidates **4c** and **4l** through low score energy values and the establishment of diverse bonding interactions with the active site residues. Finally, the ADMET profiling of the most active spiroheterocycles proved their remarkable drug-like and pharmacokinetic properties.

1. Introduction

Over the past decade, multidrug-resistant (MDR) bacteria, referred as "superbugs", have dramatically spread throughout the world and became a serious global public health emergency [1–3]. According to the World Health Organization (WHO), antimicrobial resistance has been prioritized as one of the top 10 global public health threats facing humanity [4]. The overuse and misuse of antibiotics, as well as the lack of new antimicrobial development, remain the major factors contributing to the spread and rise of MDR pathogens [5] that has slowed down the eradication process of infectious diseases. The repeated administration of antimicrobial drugs in animals or humans promotes the

* Corresponding authors.
E-mail addresses: sarra.boudriga@fsm.rnu.tn (S. Boudriga), michael.knorr@univ-fcomte.fr (M. Knorr).

https://doi.org/10.1016/j.molstruc.2024.138104
Received 27 January 2024; Received in revised form 17 March 2024; Accepted 19 March 2024
Available online 21 March 2024

dissemination and acquisition of antibiotic-resistant strains [6], thus reducing their effectiveness against infectious diseases and making them increasingly difficult or nearly impossible to treat [7]. This lowered efficacy urgently necessitates the demand for the development of novel therapeutic agents.

N-heterocycles play a crucial role in the research of new medicines, as they are recurring motifs in several commercially approved drugs and synthetic drug-like molecules [8–15]. A huge number of bioactive synthetic compounds and natural alkaloids based on spirooxindole-pyrrolidines, a subclass of *N*-spirocyclic heterocycles, are well-recognized as pivotal components in numerous bioactive natural compounds and relevant synthetic drugs [16–21]. The peculiar conformational rigidity and inherent 3D geometrical structure, imparted by the spiranic carbon, allow for outstanding binding-interactions of these spirocyclic systems with various protein receptors. This increased affinity for biotargets provides a better physicochemical properties an improved therapeutic efficacy, making them promising drug-likes [22–24]. Some illustrative examples of therapeutically relevant scaffolds containing the spirooxindole motif are shown in Fig. 1.

For example, naturally occurring Strychnofoline (**1**) (Fig. 1), extracted from the leaves of *Strychnos usambarensis*, shows very promising antimitotic activity towards Ehrlich tumor cell and cultures of mouse melanoma [25]. The synthetic spirooxindolepyrrolidines MI-888 (**2**) and MI-219 (**3**) (Fig. 1), currently in preclinical trials for cancer therapy, have been reported as potent inhibitors of MDM2–p53 protein-protein (PP) interaction [18,26,27].

Furthermore, various derivatives have been described as antiviral [20], antimicrobial [28–30], analgesic and anti-inflammatory [31], anti-acetylcholinesterase [32], anti-diabetic [33–35] and antitubercular agents [36–38].

Due to its multiple advantages in terms of enhanced operational simplicity, reaction rate, and higher yield, microwave (MW) assisted multicomponent reaction (MCR) has emerged as a powerful tool for the synthesis of spirooxindole heterocycles [39–45].This environmentally friendly approach provides a high-throughput conception of libraries of complex architectural compounds with remarkable structural diversity, unlocking novel avenues for identifying new drug-like molecules [46–48]. The capacity to achieve reaction from readily, cheap, and simple available starting materials *via* the formation of multiple chemical bonds in an one-step operation and shorter reaction time, along with facilitated work-up of the resulting products, makes microwave-assisted MCRs a synthetically robust tool for green synthesis compared toother step-by-step strategies [49–51].

On the other side, the piperidone framework is an ubiquitous motif found in several therapeutically significant alkaloids and synthetic drug-like molecules with a broad spectrum of promising biological activities such as antitumoral [52], cholinesterase inhibitory [53], anti-inflammatory [54], and antifungal activity [55] (Fig. 2).

In light of the significance of spirooxindolepyrrolidine and piperidone heterocycles in medicinal chemistry, we recently reported an unprecedented asymmetric synthesis of enantiopure dispirooxindolopyrrolidine-piperidones *via* the three-component reactions of *(E,E)*−3,5-bisarylidene-*N*-[*(S)-(-)*-methylbenzyl]−4-piperidones **1** with azomethine ylides, generated *via* thermal [1,2]-H shift of isatin-based iminoesters. The latter were formed *in situ* from the condensation of isatin **2** and glycine methyl/ethylester **3a,b** (Scheme 1A) under traditional conditions (acetonitrile, 80 °C, 2 h) [56].

Despite the efficiency of our approach, we felt a great challenge to explore the formation of these promising scaffolds under MW-assisted conditions, expecting improved yields through (*i*) shortened reaction times and (*ii*) expanding the spirooxindole structural diversity by employing another amino ester, namely sarcosine methyl ester **3c** (Scheme 1B). Such a protocol has not yet been explored for the construction of spirooxindolepyrrolidine in enantiopure form, making it a particularly challenging endeavor. Moreover, to the best of our knowledge, the secondary amino ester **3c** has received little attention as a component in the formation of azomethine ylide by [1,2]-prototropy of the corresponding isatin-derived iminoester. In order to further valorize our preparative work, we explored the pharmacological profile of the synthetized compounds which, up to now, have never been reported.

Motivated by the aforementioned information and as a continuation of our research in the domain of bioactive *N*-spiroheterocycles [31,57,

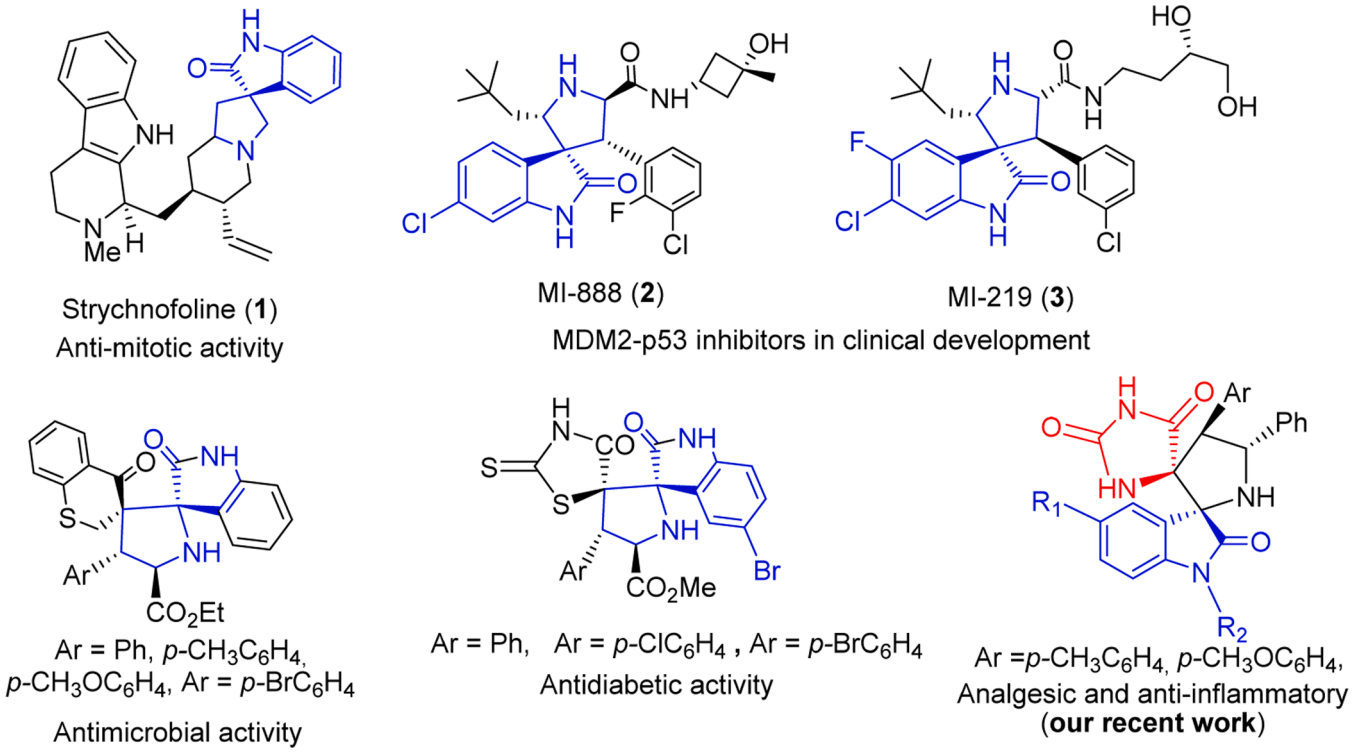

Fig. 1. Representative examples of spirooxindoles of medicinal interest.

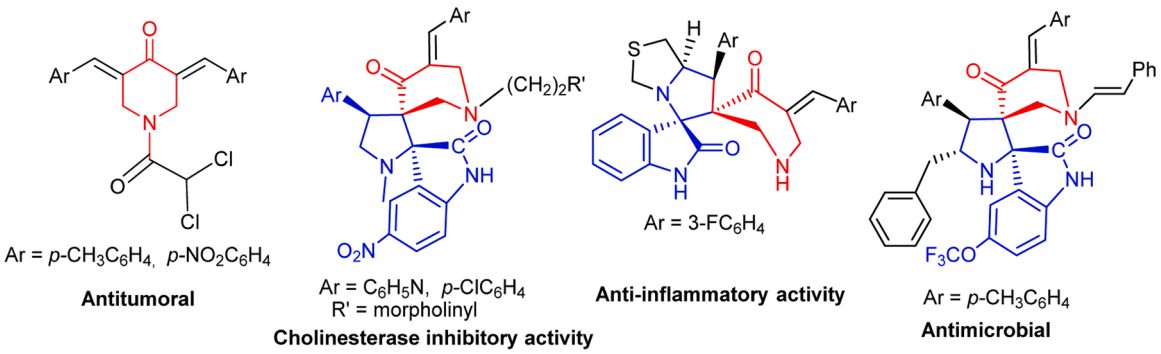

Fig. 2. Examples of biologically active piperidone scaffolds.

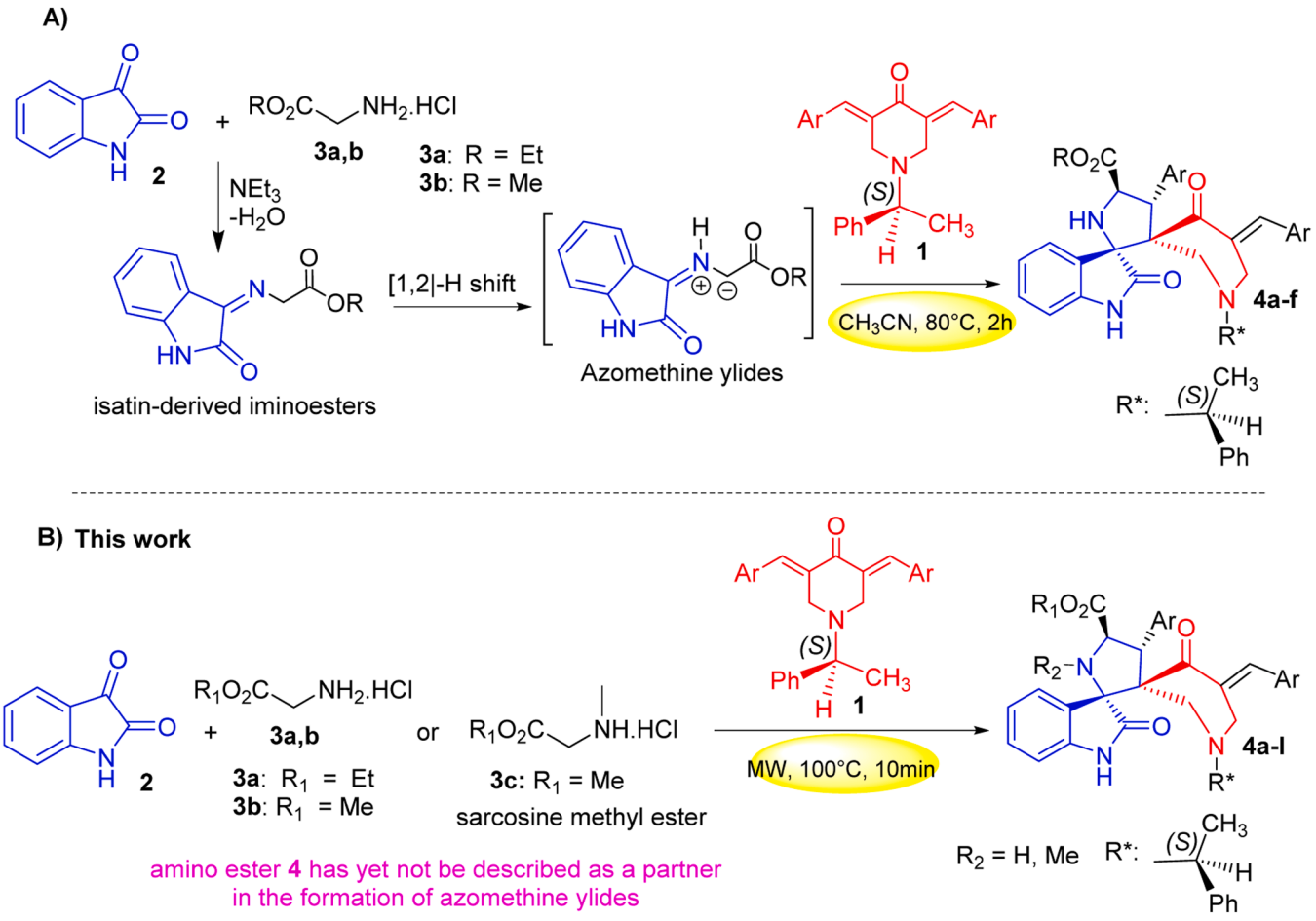

Scheme 1. (A) Our previous work of MCR [3 + 2] cycloaddition of enantiopure piperidone, isatin and aminoesters. (B) Microwave-assisted MCR with diverse primary amino ester as reaction partners (this work).

36,58,59], we report here, for the first time, the synthesis of optically active piperidone-dispirooxindolopyrrolidines by microwave-assisted multicomponent reaction (MCR) methodology, combining enantiopure *(E,E)*−3,5-bisarylidene-*N*-[*(S)-(-)*-methylbenzyl]−4-piperidones **1**, isatin **2** and *α*-aminoesters **3a-c**.

The stereochemistry of the novel *N*-spiroheterocycles derived from sarcosine methyl ester was confirmed by a single-crystal X-ray crystallography study of compound **4g**. To further valorize the synthetic results, the new scaffolds were screened *in vitro* to evaluate their antimicrobial potential. To the best of our knowledge, highly functionalized enantiopure spirooxindole-piperidones were identified for the first time as promising antimicrobial agents. Finally, to validate the bioassay results and to get an insight about the mechanism of action of the synthetized compounds, an *in silico* molecular docking study of the most potent derivatives was performed, along with an investigation of the ADMET properties [60].

2. Result and discussion

2.1. Chemistry

We started our investigation using optically active *(E,E)*−3,5-bis-benzylidene-*N*-[*(S)-(-)*-methylbenzyl]−4-piperidone **1a**, isatin **2** and chlorohydrate of sarcosine methyl ester **3c** as model substrates (Scheme

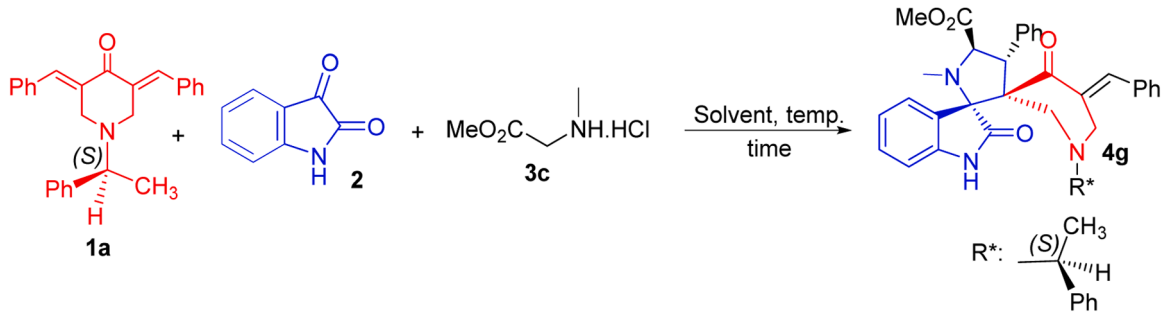

Scheme 2. Three-component 1,3-dipolar cycloaddition leading to spiropyrrolidine-fused piperidone hybrid **4g**.

2).

At the onset of our investigation, we attempted to access the targeted spirooxindole-piperidone 4 g according to a previously published procedure for the efficient synthesis of spirocyclic analogues derived from glycine methyl/ethyl ester **3a,b** [56]. For that purpose, equimolar amounts of **1a, 2** and **3c** were refluxed in acetonitrile at 80 °C for 2 h. The desired optically active **4g** ($[\alpha]_D^{25} = -123.0$ (c 0.20, $CHCl_3$)) was obtained in 55 % yield (Table 1, *entry 1*). No significant increase in yield could be achieved when increasing the reaction time from 3 to 4 h (64% *vs.* 66 % yields, respectively, *entries 2* and *3* in Table 1).

In order to reduce the reaction time and improve the yield of compound **4g**, the reaction was subjected under microwave irradiation conditions at 80 °C for 5 and 10 min in MeCN (Table 1, *entries 4* and *5*), yielding the product with 75 % and 80 % yields. The reactions were further screened with EtOH and MeOH as polar protic solvents with varying temperatures and reaction times, allowing to augment further the overall yields (Table 1, *entries 6–9*).

When conducting the reaction in MeOH at 100 °C for 10 min, 4 g was isolated in almost quantitative yield (Table 1, *entry 9*). Subsequently, the scope of the MW-assisted MCR was extended using several enantiomerically pure dipolarophiles **1** bearing electronically different substituents at the *para* position of the phenyl ring (Me, OMe, Br, Cl and NO_2). As shown in Scheme 3, this eco-friendly approach affords chiral spirooxindolopyrrolidines-fused piperidones **4 g-l** with excellent yields up to 97 % (Scheme 3).

Notably, the MCR also worked well when employing glycine methyl/ethyl esters **3a,b** as an alternative aminoester, instead of **3c**, providing the corresponding spirooxindolepyrrolidines **4a-f** in 92–97 % yields (Scheme 3). These results demonstrate the efficiency of microwave-assistance for the MCR, as it increases the yield along with a considerably reduced reaction time of 10 min compared to conventional heating conditions (72–85 % in 2 h applied for the preparation of **4a-f**). The enantiomeric purity of the compounds was checked by their specific optical rotation determined by a polarimeter.

Table 1
Optimization of the reaction parameters for the synthesis of 4g.

Entry	Solvent	Condition	Time (Min.)	Yield (%)[a]
1	CH_3CN	80 °C	120	55
2	CH_3CN	80 °C	180	64
3	CH_3CN	80 °C	240	66
4	CH_3CN	80 °C (200 W, 80 °C)	5	75
5	CH_3CN	80 °C (350 W, 80 °C)	10	80
6	EtOH	MW (350 W, 80 °C)	5	85
7	EtOH	MW (350 W, 100 °C)	10	89
8	MeOH	MW (350 W, 80 °C)	5	94
9	MeOH	MW (350 W, 100 °C)	10	97

[a] Isolated yield after recrystallization.

2.2. Spectroscopic and crystallographic characterization of cycloadducts 4

The structure and absolute configuration of the enantiopure piperidone-grafted spirooxindolepyrrolidines **4** were unambiguously deduced from both their spectroscopic data and an X-ray structure determination performed on compound **4g**. The assignments of the chemical shifts from the ^1H and ^{13}C NMR spectra of the studied compounds were based on literature data [56]. As representative example, relevant ^1H and ^{13}C chemical shifts of spirocompound **4g** are illustrated in Fig. 3.

In the ^1H NMR spectrum of **4g** (Fig. S13 in the Supplementary Materials), the protons H-5 and H-4 appear as two mutually coupled doublets at δ 4.81 and 4.97 ppm, respectively. The multiplicity and the value of the ^3J coupling constant ($J = 9.9$ Hz) of these two signals unambiguously confirm the *trans*-relationship between H-4 and H-5 protons and ascertain the regiochemistry proposed for cycloadduct **4g** in Fig. 3, which is in accordance with our earlier reports on related compounds [56]. The broadened singlet at δ 8.54 ppm is assigned to the H-1′ proton, and the two singlets at δ 2.11 and 3.66 ppm are attributable to the N—CH_3 and CH_3O protons, respectively, confirming the cycloaddition of azomethine ylide derived from sarcosine methyl ester across the dipolarophile. The multiplet in the region between 6.71–7.51 ppm indicates the presence of aromatic protons. The proton decoupled ^{13}C NMR spectrum of **4g** (Fig. S14) reveals the presence of three signals at δ 196.4, 177.4 and 171.8 ppm, attributed to the carbonyl groups of the piperidone, oxindole and ester moieties, respectively. The resonances corresponding to the two spirocarbons C-2 and C-3 are observed at δ 75.8 and δ 67.6 ppm, respectively. The carbon signals at 63.4 and 63.4 ppm can be attributed to C-5 and C-4, respectively. For the assignment of the methoxy, methyl, and spirocarbons, a DEPT-135 spectrum was recorded (Fig. S15).

The absolute configuration of the enantiopure spirooxindolopyrrolidine-piperidone stereocenters was corroborated by analysis of the single-crystal X-ray structure of hybrid **4g**. The molecular structure depicted in Fig. 4 reveals that the absolute configuration of **4g** is (*2R, 3R, 4S,* and *5S*). The Flack parameter [61] of 0.02(4) is close to 0 indicating that the absolute structure given by the structure refinement is correct for the two independent molecules **M1** and **M2** (Fig. S26).

In addition, the exocyclic double bond of 4-piperidone and the chiral auxiliary (-NMePh) are oriented *pseudo*-equatorially and adopt a half-chair conformation. This diastereofacial selectivity can be explained by the *exo*-approach of the *(Z,E)*-azomethine ylide on the less hindered upper face of the exocyclic alkenes. The stereochemistry of the tetracyclic core, bearing three additional aryl groups at C2, C10 and C1, is in the solid state in line with the NMR data in solution and establishes the transoid arrangement of two the hydrogen atoms attached to C2 and C3 of the pyrrolidine-type five-membered cycle.

The asymmetric unit of **4g** shown in Fig. S26 contains two independent molecules (with slightly different bond lengths and angles), crystallizing in the monoclinic space group $P2_1$. Within the crystal, both

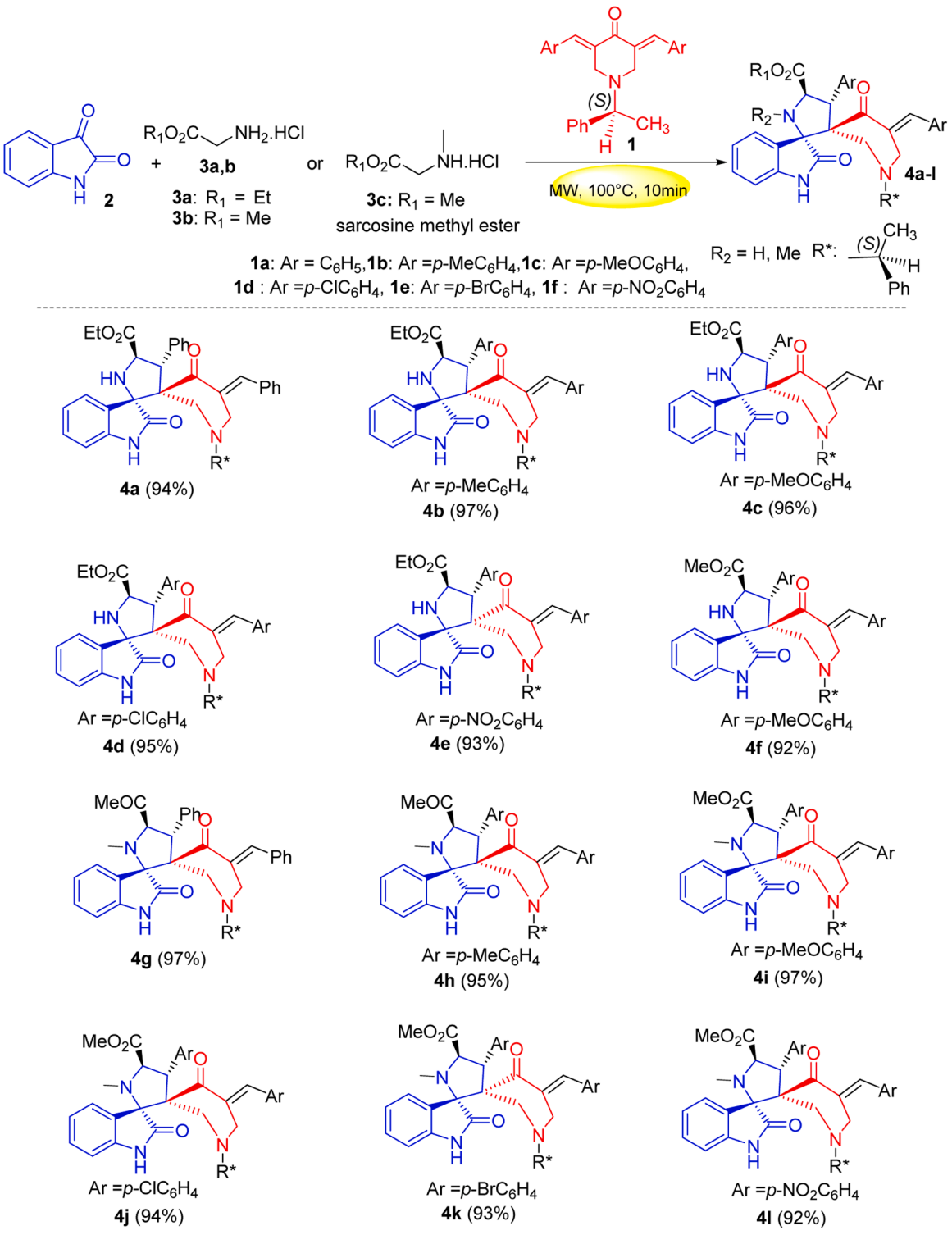

Scheme 3. Synthesis of enantiopure spirooxindolopyrrolidine-piperidones **4a-l**.

molecules **M1** and **M2** are interconnected through intermolecular N–H···O and C–H···O hydrogen bonding forming monodimensional supramolecular M1···M1···M1 and M2···M2···M2 arrays (Fig. 5). There are no significative contacts between the **M1** and **M2** molecules. Fig. 5 shows that in the M1 chain each molecule forms an interaction occurring between N2–H2 and O2 with *d*(N2-H2····O4)12.35(3) Å, the N2–H2····O4 angle being 152(2)°. Furthermore, a second weak intermolecular hydrogen bond occur between C34–H34 and O4 (*d* (C34–H34····O42 2.41 Å)).

To better clarify the presence of weak intermolecular contacts occurring in the crystalline state, that may be complementary and relevant to the docking simulation shown in Section 2.4, a Hirshfeld surface analysis [62] was carried out utilizing the CrystalExplorer21 software package by Spakman et al. [63]. For heterocycle **4g**, two independent Hirshfeld surfaces are mapped over d_{norm} in the ranges from –0.2845 to 1.7544 and –0.3071 to 1.7398 (both arbitrary units).

As shown in Fig. 6, the red spots on the isosurface highlight the strong intermolecular interactions. Overall, several strong N–H···O

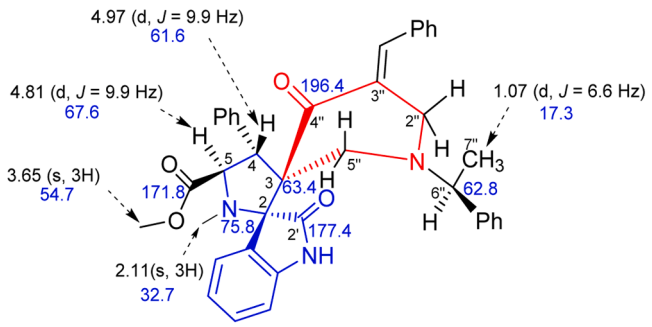

Fig. 3. ^{1}H (black) and ^{13}C NMR (blue) chemical shifts and coupling constants of **4g**.

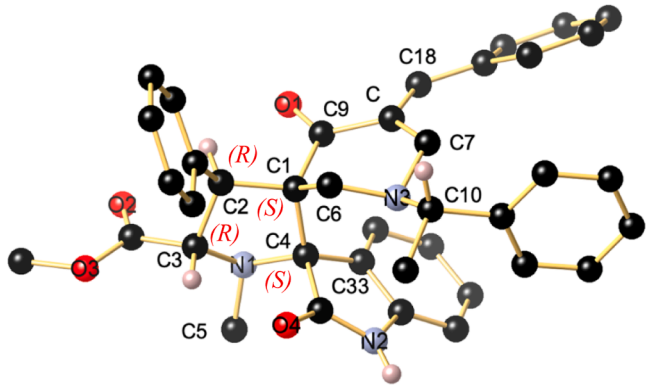

Fig. 4. Ball and Sticks presentation of the molecular structure of 4 g in the crystal. For clarity, only stereochemically significant hydrogen atoms are shown. Only one of the two independent molecules in the unit cell is presented (M1). Selected bond lengths (Å) and angles (°): C3–N1 1.454(2), C4–N1 1.467 (2), C4–C1 1.585(2), C1–C2 1.572(2), C2–C32 1.546(2), C1–C6 1.536(2), C6–N3 1.459(2), N3–C7 1.456(2), N3–C10 1.491(2), C7–C8 1.499(2), C8–C18 1.343(2), C8–C9 1.499(2), C9–O1 1.216(2), C9–C1 1.542(2), C4–C39 1.566(2), C39–O4 1.223(2), C39–N2 1.375(2), N2–C38 1.401(2), C38–C33 1.369(2); C1–C2–C3 104.67(12), C2–C3–N1 103.05(120), C3–N1–C4 106.91(13), N1–C4–C1 101.62(12), N1–C4–C39 113.06(14), C1–C6–N3 108.89(13), C6–N3–C7 101.47(10), C7–C8–C18 1231.35(14), N3–C7–C8 113.09(13), N3–C10–C11 114.703(14), C39–N2–C38 111.53(15), C4–C39–N2 108.40(15).

contacts and weaker N–H···O contacts can be detected, what can be inferred from the respective fingerprint plots (Fig. S27).

2.3. Biological evaluation of the synthesized heterocycles

The optically active dispirooxindole derivatives **4** were evaluated for their antibacterial activity against multiple bacterial strains (*Pseudomonas aeruginosa* ATCC 9023, *Escherichia coli* ATCC 25,922, *Salmonella enterica* 800,390 and *Bacillus subtilis* ATCC 6633), and a pathogenic reference yeast namely *Candida albicans* ATCC 90,028.

The *in vitro* antimicrobial activity of the novel dispiropyrrolidines was assessed by the determination of the minimal inhibitory concentration (MIC) using the micro dilution method, as described by Rattan [64]. The results are summarized in Table 2. To compare and to evaluate the potency of the tested derivatives, Ampicillin and Griseofulvin were chosen as antibacterial and antifungal references, respectively. As shown in Table 2, almost all synthesized analogues were found to be more active against highly resistant *P. aeruginosa* with MIC values of 12.1 μg/mL, compared to the standard drug Ampicillin (MIC=100 μg/mL). The only exceptions are compounds **4b** (MIC = 125 μg/mL) and **4g** (MIC= 250 μg/mL).

With regard to *E. coli*, a potent activity was ascertained for all compounds, except for hybrid **4b**, when compared to Ampicillin (MIC=100 μg/mL). Notably, the best activity was obtained for compounds **4c** and **4f** with a MIC value of 12.1 μg/mL, followed by **4d, 4k**, and **4l** with a MIC value of 31.25 μg/mL. We also noticed that heterocycle **4c** exhibits strong antibacterial activity against *S. enterica* bacteria with a MIC value of 12.1 μg/mL, in comparison with Ampicillin (MIC=250 μg/mL).

However, compounds **4a, 4d** and **4j**, with MIC values of 250 μg/mL present an activity comparable to that of the reference antibiotic. Remarkably, hybrid **4e** (MIC = 64 μg/mL) is more potent than Ampicillin (MIC = 100 μg/mL) against *B. subtilus*. In addition, derivatives **4a, 4c, 4d** and **4j-l** with a MIC value of 100 μg/mL demonstrate activity against *B. subtilus* similar to that of the reference antibiotic Ampicillin (MIC = 100 μg/mL).

On the other hand, the *in vitro* antifungal activity data reveal that **4a-c** display improved activity with a MIC value of 250 μg/mL compared to Griseofulvin (MIC = 500 μg/mL), followed by compounds **4d** and **4k** (MIC = 325 μg/mL). The remaining derivatives showed only moderate antifungal properties.

2.4. Computational approach

To get an insight about the mechanism of action of series **4**, we docked the most antibacterial derivatives *i.e.*, **4c, 4k, 4j** and **4l** into the binding sites of the following bacterial receptors: multiple virulence factor regulator (MvfR) (PDB ID 4JVI) from *P. aeruginosa* [65], Topoisomerase IV (PDB ID 3FV5) from *E. coli* [66], RamR (PDB ID 6IE9) *S. enterica* [67], and heterologous protein expression (PDB ID 2RHL) from *B. subtilis* [68]. They were also docked into the secreted aspartic protease target (PDB ID 3Q70) from *C. albicans* [69].

2.4.1. Molecular docking approach for the antibacterial proteins

The docking poses of the test molecules revealed their ability to bind to the active site residues of the enzyme through several types of interactions. This was further confirmed by significant binding energy, as reflected by the lower docking score (S-score) values.

*2.4.1.1. Orientation and bonding interactions of compounds **4c, 4k, 4j** and **4l** in the pocket site of mvfr (Multiple virulence factor regulator; PDB ID 4JVI).* The results of the best poses for compounds **4c, 4k, 4j** and **4l** against MvfR PDB ID 4JVI) from Gram-negative *P. Aeruginosa* (https://en.wikipedia.org/wiki/Pseudomonas_aeruginosa) TMK (ID: 4QGG) are listed in Table S1. Molecular docking results confirm that all candidates **4c, 4k, 4j** and **4l** had the highest negative score values of (−6.892, −6.656, −6.458, and −6.732 kcal/mol respectively), compared to the standard drug Ampicillin with a score of −5.187 kcal/mol (Table S1).

Comparatively, compounds **4c** and **4l** were the most active against the antibacterial agents towards *P. aeruginosa* (MvfR) (PDB ID 4JVI), indicating that they form a similar number of interactions with the MvfR protein of *P. aeruginosa* as Ampicillin, but there are small differences in residue types (Table –S1). Compound **4c** forms a strong [70,71] hydrogen bond with crucial residue LEU207 (2.32 Å) of the *P. aeruginosa* MvfR protein (Table –S1 and Fig.7(a)).

Moreover, this candidate exhibits nine hydrophobic interactions with the binding site of the MvfR target: a π-π-stacked interaction was evidenced between TYR258 and the 6-membered aromatic ring of compound **4c** (distance: 4.33 Å).

In addition, ALA190, LEU207, ILE263 and VAL211 form alkyl-type hydrophobic interactions with compound **4c**. Four other π-alkyl hydrophobic interactions were also observed (Table S1 and Fig.7(a)).

It is evident that molecule **4l** forms only one strong hydrogen bond with the binding site residues of the MvfR protein. LEU207 forms a hydrogen bond (bond distance = 2.33 Å) with the hydrogen atom of molecule **4l** ((Table S1 and Fig.7(d)). Furthermore, the same molecule forms 14 hydrophobic interactions with ten residues of the MvfR target, namely TYR258, ALA190, LEU207, ILE263, LEU197, LEU208, ILE236,

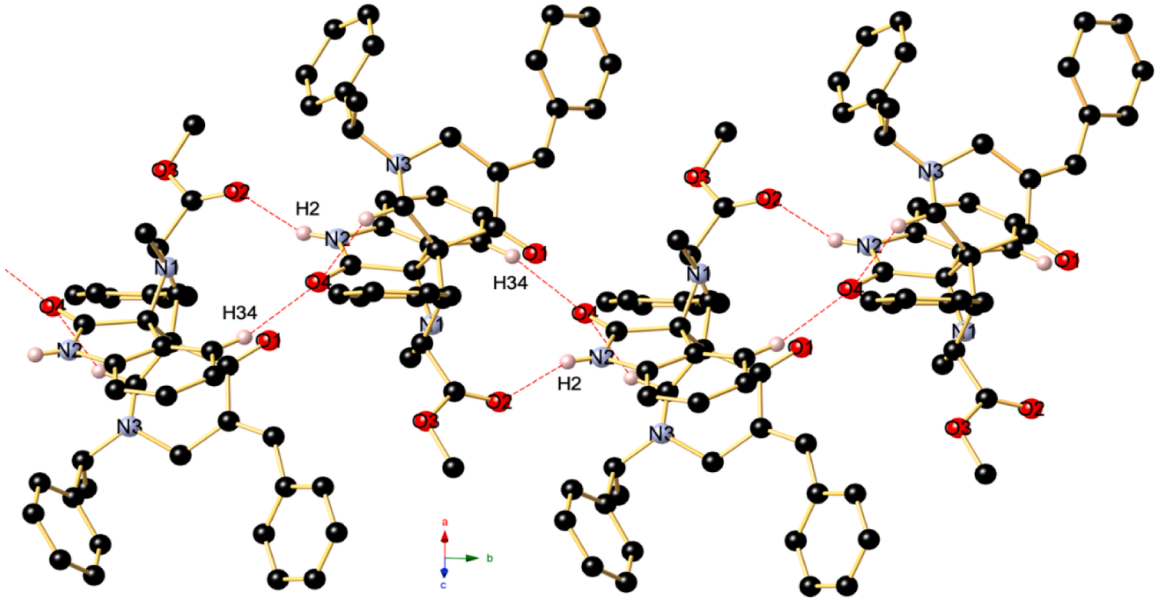

Fig. 5. Association of the M1 molecules in the packing through intermolecular N–H···O and C–H···O hydrogen bonding forming a supramolecular 1D array running along the *b* axis.

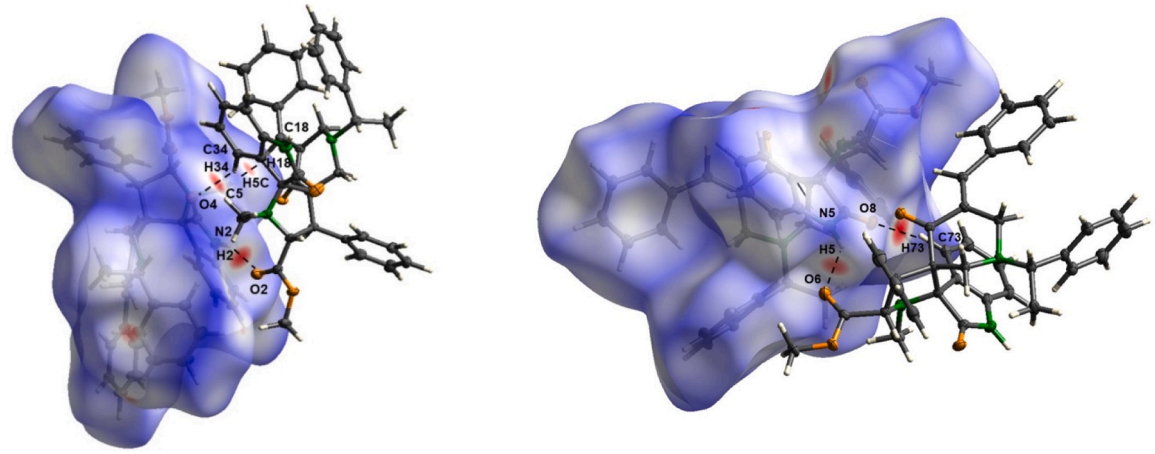

Fig. 6. (left) Hirshfeld-surface of M1, intermolecular bonding between two M1 molecules −0.2845 to 1.7544 a. u. (right) Hirshfeld-surface of M2, intermolecular bonding between two M2 molecules −0. 0.3071 to 1.7398 a. u.

Table 2
Antibacterial and antifungal activities of compounds 4 (MIC was determined in µg/mL).

Compound	P. aeruginosa ATCC 9023	E. coli ATCC 25,922	S. enterica 800,390	B. subtilus ATCC 6633	C. albicans ATCC 90,028
4a	36	100	250	100	250
4b	125	125	500	125	250
4c	12.1	12.1	12.1	100	250
4d	12.1	31.25	250	100	329
4e	12.1	36	500	64	500
4f	12.1	12.1	1000	1000	1000
4 g	250	100	500	125	500
4h	12.1	36	500	500	500
4i	12.1	36	500	500	500
4j	12.1	36	250	100	500
4k	12.1	31.25	500	100	329
4l	12.1	31.25	500	100	500
Ampicillin	100	100	250	100	–
Griseofulvin	–	–	–	–	500

VAL170, LEU189, and VAL211. In this context, recent investigations [70,72] proved that LEU207, ILE236 and YR258 play a fundamental role in the inhibition of the MvfR receptor.

*2.4.1.2. Orientation and bonding interactions of compounds **4c, 4k, 4j** and **4l** in the residues site of topoisomerase iv (PDB ID 3FV5).* Based on the score energy values, candidates **4c** and **4l** were shown to be the most potent Topoisomerase IV receptor inhibitors among the studied candidates (compared to **4j** and **4k**). This was confirmed by their high affinity to the pocket site of the *E. coli* target (PDB ID 3FV5). The complexes formed by these candidates exhibited lower score energy values of −6.272 and −5.546 Kcal/mol, respectively, conferring them the highest negative score values, comparable to Ampicillin (the standard drug) with a score of −4.576 kcal/mol (Table S2). On the other hand, compound **4c** forms only one strong hydrogen bond with the binding site of the Topoisomerase IV target. ASP69 forms a hydrogen bond with the hydrogen atom of compound **4c** (bond distance = 2.74 Å) (TableS24 + Fig. 8(a)).

Furthermore, this compound established one electrostatic

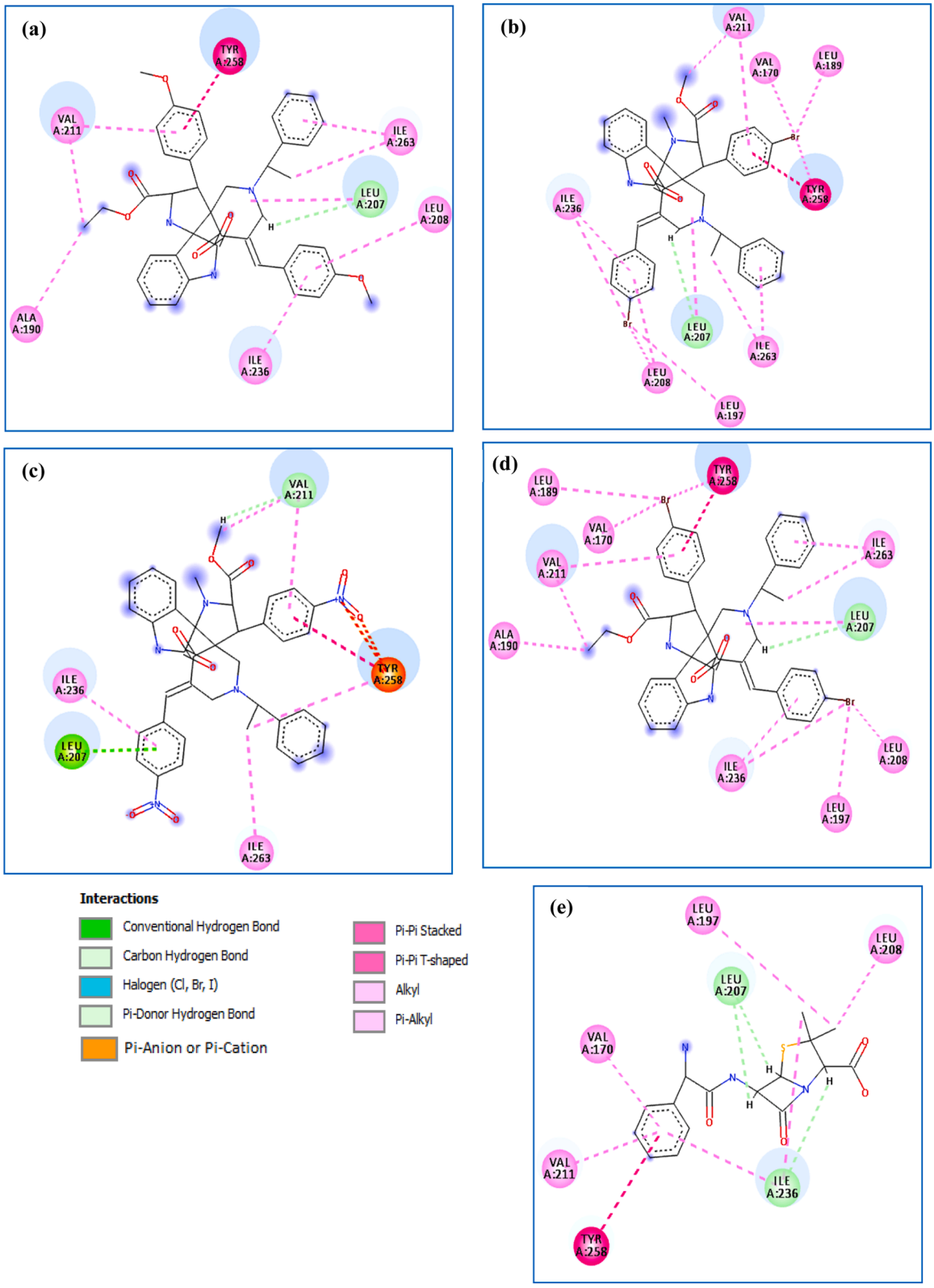

Fig. 7. 2D diagram of interactions of the compounds: (a):**4c**, (b): **4j**, (c): **4k**, (d): **4l**, and (e): Ampicillin with the binding site of MvfR (PDB ID 4JVI).

interaction with GLU46 (pi-Anion) and three hydrophobic interactions with the residues HIS79, MET74, and ILE90 of the Topoisomerase IV target. Moreover, we clearly observed that compound **4l** forms three strong hydrogen bonds within the pocket of the Topoisomerase IV protein: ARG132 establishes a strong conventional hydrogen bond with the hydrogen atom of compound **4l** (bond distance = 2.61 Å). Two other strong carbon hydrogen bonds (bond distance = 2.74 and 2.93 Å) were observed between this compound and ASP77. Additionally, compound **4l** showed three electrostatic interactions with residue ARG72 and four hydrophobic interactions with residues: MET74, HIS79 and PRO75 (Table S2 and Fig. 8 (d)). These results are supported by several published papers [73,74], which mention that residues ARG72, MET74 and

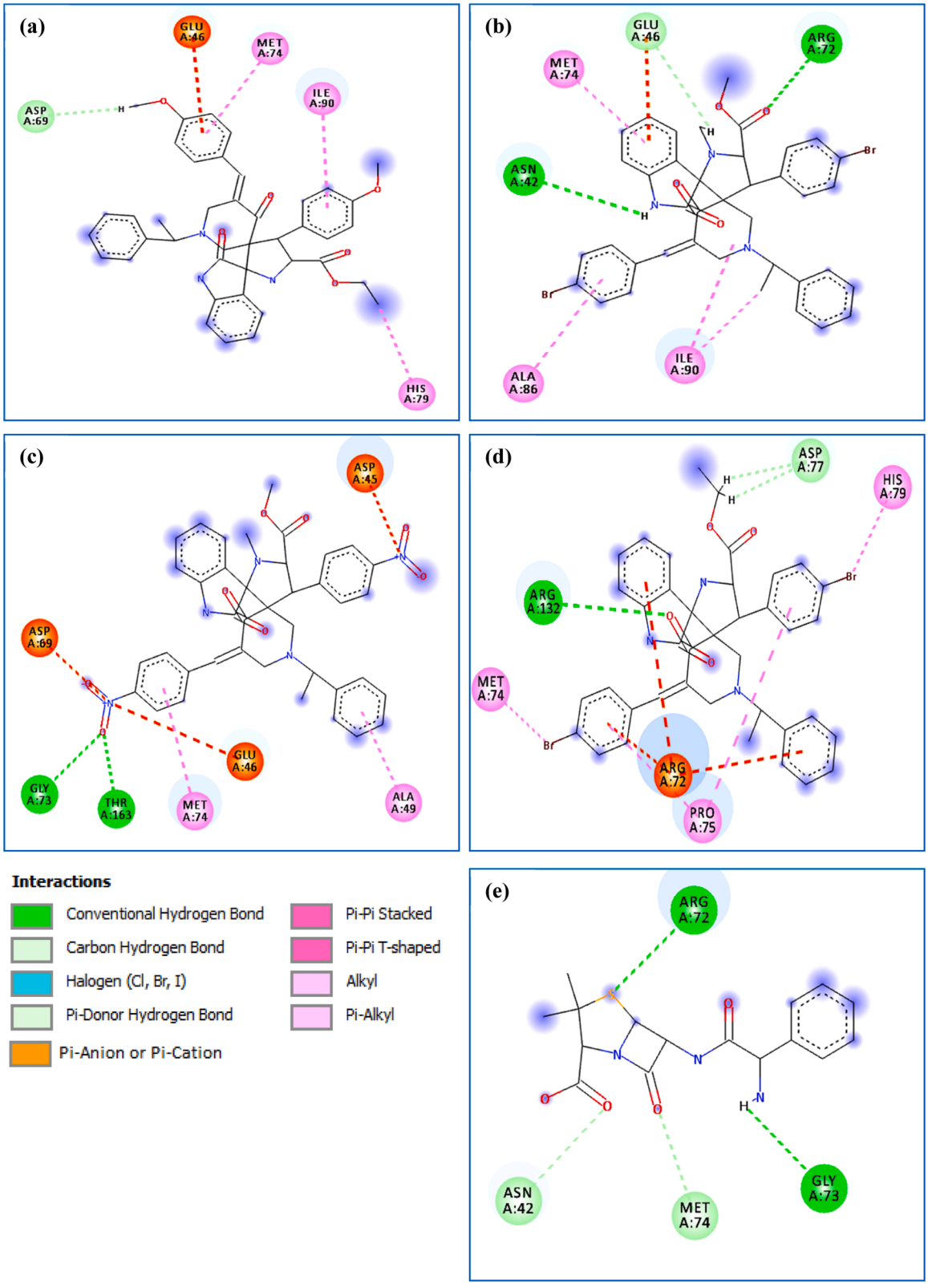

Fig. 8. 2D diagram of interactions of the compounds: (a): **4c**, (b): **4j**, (c): **4k**, (d): **4l**, and (e): Ampicillin with the binding site of Topoisomerase IV (PDB ID 3FV5).

ASN42 represent the main keys for the formation of different types of candidate interactions.

*2.4.1.3. Orientation and bonding interactions of compounds **4c, 4k, 4j** and **4l** in the binding site cavity of RamR (PDB ID 6IE9).* The docking investigations were also extended to RamR, a transcriptional repressor of the gene-encoding RamA protein, which controls the expression of the multidrug efflux system genes acrAB-tolC [75]. The docking results show that the most efficient compounds **4c** and **4l** against the RamR target (PDB ID 6IE9) present good docking score energies values of

−9.286 and −8.449 kcal/mol, respectively (Table S3).

They form numerous interactions with the enzyme RamR of *S. enterica* (PDB ID 6IE9) compared to a score energy of −6.482 kcal/mol of the standard drug Ampicillin. Compound **4c** establishes 8 strong hydrogen bonds, including three conventional hydrogen bond types with residues ARG131 and ARG148 (distances: 2.99, 1.75 and 2.22 Å), and five carbon hydrogen bonds with residues LYS63, PHE127, ALA123 and CYS134 (distances: 2.51, 2.72, 2.37, 2.93 and 2.95 Å, respectively). Additionally, this compound forms three electrostatic interactions with residues LYS63, ARG136 and ASP152. Furthermore, 9 hydrophobic interactions were established between compound **4c** and the following residues: TYR92, PHE155, LEU66, CYS67, MET70, ILE88, ARG136 and LEU139 (Table S3 + Fig. 9(a)). We also noticed that compound **4l** fits well into the pocket site of the RamR target (PDB ID 6IE9), forming two

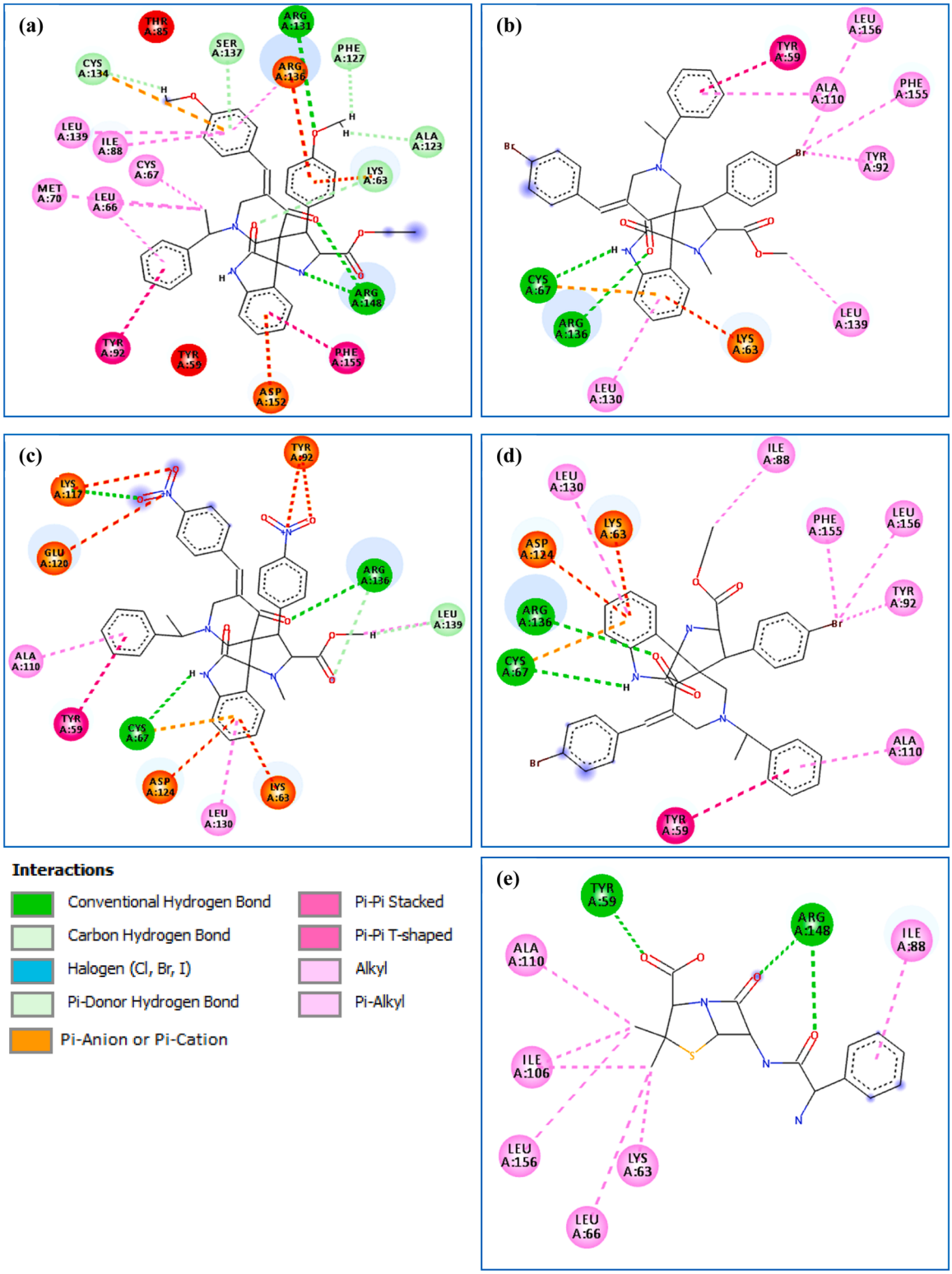

Fig. 9. 2D diagram of interactions of the compounds: (a):**4c**, (b):**4j**, (c):**4k**, (d):**4l**, and (e): Ampicillin with the binding site of RamR (PDB ID 6IE9).

strong conventional hydrogen bonds with residues ARG136 and CYS67 (distances: 2.41 and 2.69 Å). In addition, there are two electrostatic interactions with residues: LYS63 and ASP124. Furthermore, 7 hydrophobic interactions were observed between compound **4l** and residues TYR59, LEU156, ILE88, TYR92, PHE155, LEU130, and ALA110 (Table S3 + Fig. 9(d)). Other prior studies [76,77] have identified the importance of two residues in the RamR enzyme pocket (PDB ID 6IE9): ARG148 and LYS63.

*2.4.1.4. Orientation and bonding interactions of compounds **4c, 4k, 4j** and **4l** in the binding site cavity of heterologous protein expression (PDB ID 2RHL).* According to the score energy values, candidates **4c** and **4l**

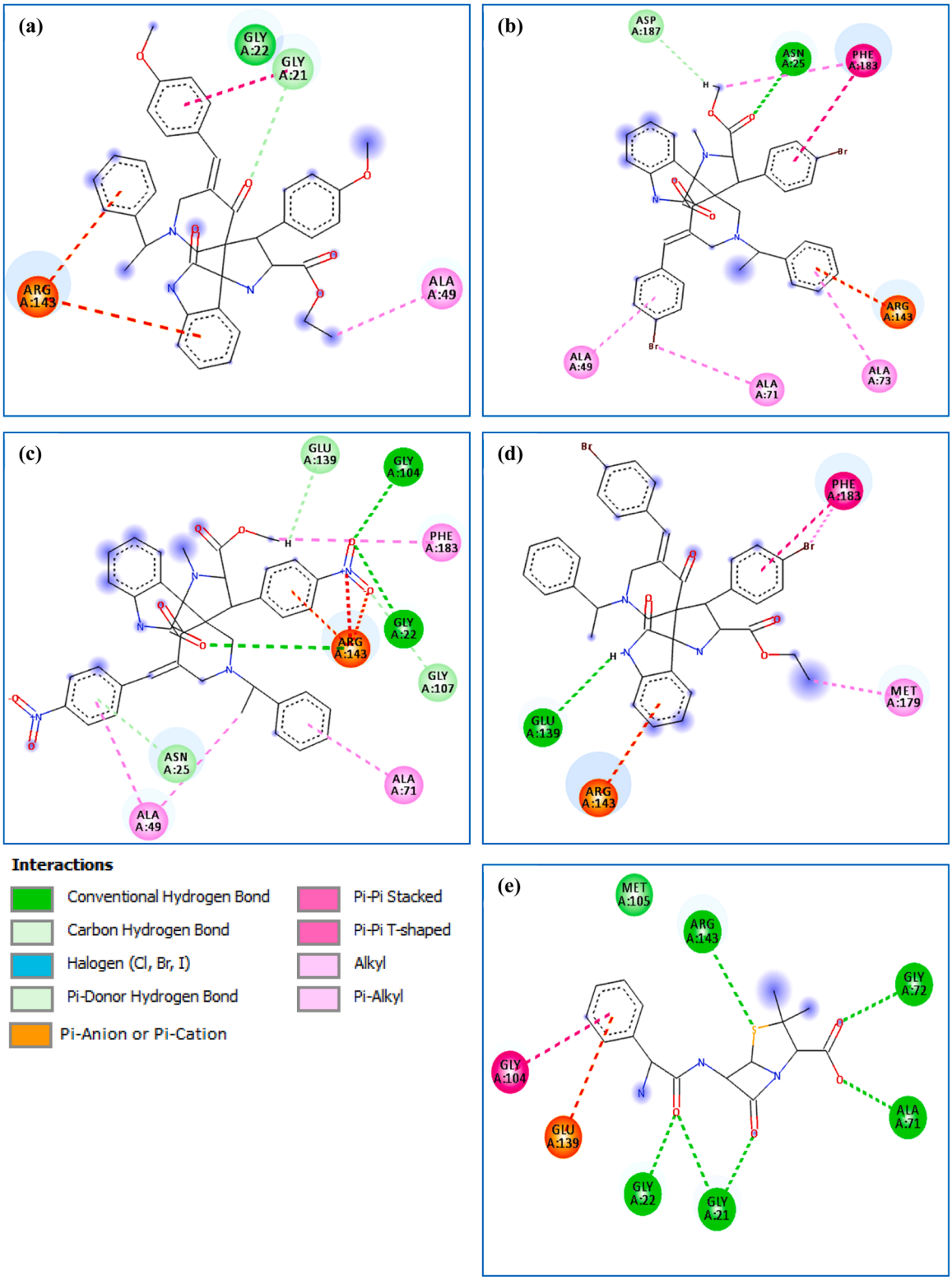

Fig. 10. 2D diagram of interactions of the compounds: (a):**4**c, (b):**4j**, (c):**4k**, (d):**4l**, and (e): Ampicillin with the binding site of Heterologous protein expression (PDB ID 2RHL).

showed high affinity for Heterologous protein expression (PDB ID 2RHL). The complexes established by these two candidates had the lowest score energy values of −6.997 and −6.875 Kcal/mol, respectively, compared to other complexes formed by compounds **4j** and **4k**, and with Ampicillin with an energy value of −5.451 kcal /mol (Table S4).

The results obtained indicate that compound **4c** forms a stable complex with the pocket of *B. subtilis* (PDB ID: 2RHL), characterized by the formation of only one strong carbon hydrogen bond between the oxygen atom of the candidate and GLY21 at a distance of 2.71 Å. Two other electrostatic interactions occur between compound **4c** and residue ARG143. This compound forms two hydrophobic interactions with

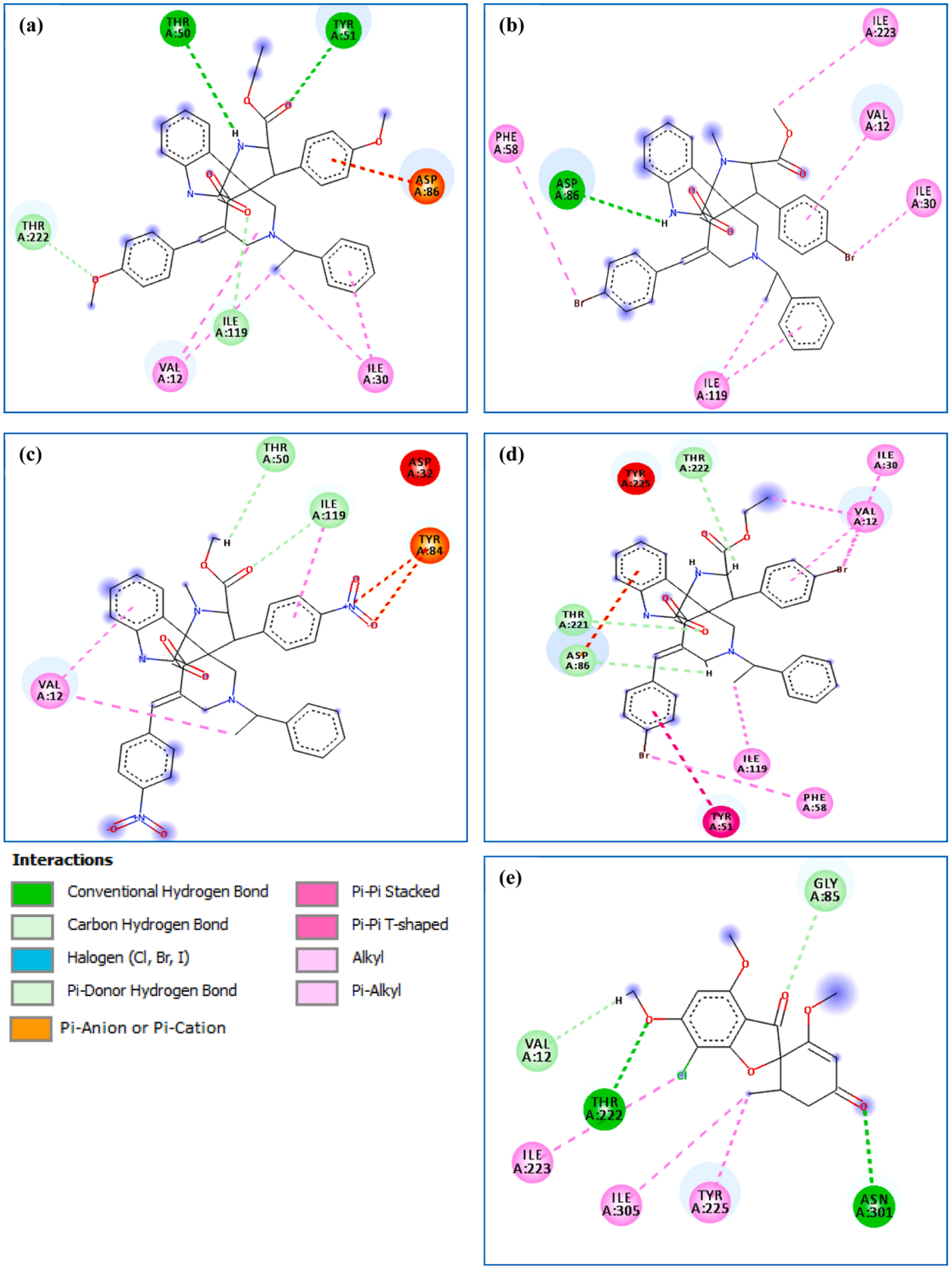

Fig. 11. 2D diagram of interactions of the compounds: (a):**4c**, (b):**4j**, (c):**4k**, (d):**4l**, and (e): Griseofulvin with the binding site of secreted aspartic protease (PDB ID 3Q70).

residues: GLY21 and ALA49 (Table S4 and Fig. 10 (a)). In contrast, we found that molecule **4l** establishes one strong conventional hydrogen bond with GLU139 (distance: 2.82 Å), and forms one electrostatic interaction with ARG143. Additionally, this compound forms three hydrophobic interactions with residues PHE183 and MET179 (Table S4 + Fig. 10(d)). Note that the present results are corroborated by prior studies [78,79] indicating that inhibition of *B. subtilis* target (PDB ID:2RHL) might be dependent and crucial for their potent antibacterial activity.

*2.4.1.5. Orientation and bonding interactions of compounds **4c, 4k, 4j** and **4l** in the pocket site of secreted aspartic protease (PDB ID 3Q70).* As shown in Table S5, compounds **4c, 4k, 4j** and **4l** fit well with the binding site of the secreted aspartic protease target (PDB ID 3Q70) (https://en.wikipedia.org/wiki/Aspartic_protease). Notably, compounds **4c** and **4l** had the highest negative energy values against the secreted aspartic protease receptor (PDB ID 3Q70) (negative energy: values were −7.708 and −6.988 Kcal/mol, respectively), compared to compounds **4j, 4k** and the standard drug Griseofulvin with a score energy of −5.169 kcal/mol (Table S5). Compound **4c** forms 4 strong hydrogen bonds with the binding site of *C. albicans* target (PDB ID: 3Q70). Two conventional hydrogen bond types are formed between **4c** and residues TYR5 and THR50 (distances = 2.45 and 2.82 Å, respectively). Two additional carbon hydrogen contacts are established with residues ILE119 and THR222 (distances = 2.31 and 2.63 Å, respectively). One electrostatic interaction occurs with ASP86. Moreover, 4 hydrophobic interactions are established with residues VAL12; and ILE30 (Table S5 + Fig. 11(a)).

The docked conformation of compound **4l** in the binding site cavity of the secreted aspartic protease target (PDB ID 3Q70) forms three strong hydrogen bonds with residues THR221, ASP86, and THR222 (bond distances = 2.46, 2.36, and 2.84 Å, respectively). Furthermore, an electrostatic interaction is formed between this derivative and residue ASP86.

On the other hand, candidate **4l** establishs 7 hydrophobic interactions with the following residues in the pocket site of *C. albicans* target (PDB ID: 3Q70): TYR51, ILE119, VAL12, ILE30 and PHE58 (Table S5 + Fig. 11(d)). It is worth mentioning that these findings are supported by several studies [80,29] which reported that THR222, ASP86 and VAL12 play a crucial role in inhibiting the *C. albicans* receptor (PDB ID: 3Q70).

2.4.1.6. Physiochemical properties evaluation and ADME-Toxicity predictions. To take into account the toxicity of the compounds, ADME-T (or ADMET) predictions and physicochemical properties calculations were performed [60]. A Drug-likeness evaluation of the four candidates **4c, 4k, 4j** and **4l** was carried out using the SwissADME (http://www.swissadme.ch/, accessed on 20 October 2023) online server and pkCSM (http://biosig.unimelb.edu.au/pkcsm/prediction, accessed on 20 October 2023). All results are presented in Table 3.

According to the table, the TPSA values of compounds: **4c, 4j** and **4l** are all less than 140 Å, except for compound **4k**. In addition, all compounds contain <5 hydrogen bond donors (n-HD: (0~5)) and <10 hydrogen bond acceptors (n-HA: (0~10)). However, the spiroheterocyles have molecular weights greater than 500 g/mol, and their of MLogP and WLogP values are less than 5, except for the two compounds **4j** and **4l** having WLogP values greater than 5.

In addition, the nROTB values are <11, indicating the flexibility of the tested candidates. Preliminary analysis of these results indicated that all the criteria of drug-likeness are satisfied by the heterocycle **4c** without any violation of the Lipinski, Veber and Egan's rules [81]. Moreover, compounds **4j** and **4l** match without any violation with the Veber and Egan rules but do not fit with the Lipinski rule. In contrast, compound **4k** did not satisfy any of the Lipinski, Egan and Veber rules of 5.

From the data presented in Table 3, it can be inferred that: (*i*) The Caco-2 values of all compounds are greater than −5.15 cm/s, indicating good permeability. Notably, the HIA values of compounds **4c, 4k, 4j**, and **4l** (100, 93.12, 94.62, and 92.71 %, respectively) exceed 70 %, suggesting that these compounds can be readily absorbed orally from the gastrointestinal system into the bloodstream.

(*ii*) All compounds can penetrate the CNS as confirmed by logPS values ranging from: −3<logPS<−2. Furthermore, the logBB values of compounds (**4c, 4k, 4j** and **4l**) were: −0.73, −0.66, −0.68, and −0.72, respectively, indicating that all compounds were poorly distributed in the brain (logBB< −1) (Table 3). (*iii*) The data in this table may indicate that not all compounds are inhibitors of CYP1A2 and CYP2C19 isoforms and CYP2D6 substrate. Furthermore, none of the candidates are likely to be OCT2 (Organic Cation Transporter 2) substrates [82]. Moreover, one can clearly see that these heterocycles have an average excretion clearance (<5 ml /min /kg). Furthermore, these spiro-compounds did not exhibit AMES toxicity, except compound **4k**. However, the

Table 3
ADME-Toxicity and drug-likeness properties of the candidates 4c, 4k, 4j and 4l.

Entry	TPSA Å2	n-ROTB	MW	MLog P WLog P	n-ON acceptors	n-OHNH donors	Lipinski's violations	Veber violations	Egan violations
	<140	<11	<500	≤5	<10	<5	≤1	≤1	≤1
4c	106.20	9	671.78	3.07 4.01	8	2	Accepted	Accepted	Accepted
4j	78.95	6	769.52	4.80 5.47	6	1	Rejected	Accepted	Accepted
4k	170.59	8	701.72	2.13 3.76	10	1	Rejected	Rejected	Rejected
4l	87.74	7	769.52	4.80 5.52	6	2	Rejected	Accepted	Accepted

ADME-T	Absorption		Distribution		Metabolism			Excretion		Toxicity	
	Caco2 (10–6 cm/s)	HIA %	CNS (log PS)	BBB (log BB)	CYP1A2 inhibitor	CYP2C19 inhibitor	CYP2D6 substrate	Renal OCT2 substrate	Total Clearance (mL/min/kg)	AMES toxicity	hERG I and II Toxicity
4c	1.039	100	−2.71	−0.73	NO	NO	NO	NO	0.50	NO	NO
4j	0.923	93.12	−1.25	−0.66	NO	NO	NO	NO	0.21	NO	NO
4k	0.398	94.62	−1.89	−0.68	NO	NO	NO	NO	−0.21	YES	NO
4l	0.862	92.71	−1.34	−0.72	NO	NO	NO	NO	0.41	NO	NO

Caco-2: Colon adenocarcinoma, HIA: Human intestinal absorption, CNS: Central Nervous System permeability, BBB: Blood–Brain Barrier permeability. Caco-2: Colon adenocarcinoma, HIA: Human intestinal absorption, CNS: Central Nervous System permeability, BBB: Blood–Brain Barrier permeability, Renal OCT2 substrate: Organic cation transporter 2, hERG: Human Ether-à-go-go-Related Gene. TPSA: Topological Polar Surface Area, n-ROTB: Number Of Rotatable Bonds, MW: Molecular Weight, MLogP: logarithm of partition coefficient of compound between *n*-octanol and water, n-ON acceptors: Number of hydrogen bond acceptors, n-OHNH donors: Number of hydrogen bonds donors.

compounds examined were neither hERG I nor hERG II inhibitors (https://en.wikipedia.org/wiki/HERG).

2.4.1.7. Prediction toxicity risk. OSIRIS Property Explorer [83] was employed to evaluate the toxicity risk of side effects, such as: mutagenic, tumorigenic, irritant, and reproductive effects, as well as drug-related properties such as solubility, drug likeness, and drug score. The results of toxicological pathways of the selected compounds **4c, 4k, 4j** and **4l** are listed in Table 4.

According to Table 4, only compound **4c** has a higher risk of reproductive effect. Additionally, compounds **4j** and **4l** present a moderate risk of reproductive effect, whereas compound **4k** is deemed safe with no expected side effects. According to the results, compound **4k** does not present any toxicity concerns. Furthermore, the highest drug score value indicates that compounds **4c** and **4k** demonstrate effectiveness and potential as new drug candidates. Interestingly, the drug-likeness values of compounds **4c, 4k, 4j** and **4l** were significant, showing the following values: 4.06, 4.07, 4.26 and 2.18, respectively. As shown in Table 4, all compounds display low mutagenic, tumorigenic, and irritation risks. However, *in silico* predictive analysis with OSIRIS Property Explorer showed that all compounds exhibit good solubility.

3. Conclusions

In conclusion, we have achieved a microwave-assisted one-pot synthesis of optically active structurally diverse tetracyclic dispirooxindolopyrrolidine-piperidones using enantiopure *(E,E)*−3,5-bisarylidene-*N-[(S)-(-)*-methylbenzyl]−4-piperidones, isatin and *α*-amino esters. Compared to traditional methods, microwave-assisted asymmetric synthesis produces higher yields (up to 97 %) and requires less time (10 min). Interestingly, *N*-heterocycles **4c, 4k, 4j** and **4l** displayed promising *in vitro* antimicrobial activity.

Molecular docking methods confirmed that all compounds (**4c, 4k, 4j** and **4l**) have high affinity for the binding sites of bacterial and fungal targets, as explained by low score energy values and the formation of several types of bonds with the active site residues of selected targets. These results were compared with those of the standard drugs Ampicillin and Griseofulvin, as antibacterial and antifungal agents, respectively. Additionally, the ADMET evaluation and physic-chemical properties calculation, demonstrate that compound **4c** respects all the Lipinski, Veber, and Egan rules, indicating its potential as a drug candidate.

4. Materials and methods

4.1. Apparatus and general information

The NMR (300 MHz for ^{1}H NMR, 75 MHz for ^{13}C{^{1}H}) spectra were recorded on Bruker Avance 300 machine (Rheinstetten, Germany). The chemical shifts δ were reported in ppm relative to tetramethylsilane (TMS). Data were described as follows: chemical shift (δ in ppm), multiplicity (*s* = singlet, *d* = doublet, *m* = multiplet, *t* = triplet), coupling constants (Hz) and integration. Specific optical rotations were determined by a Perkin Elmer polarimeter. Elemental analyses were performed on a Perkin Elmer 2400 Series II Elemental CHNS analyzer (Waltham, MA, USA). Thin-layer chromatography (TLC) was performed on silica gel plates (Merck, silica gel 60 F254 0.2 mm, 200_200 nm) (Darmstadt, Germany) using UV light at 254 nm. Microwave-assisted synthesis was carried out in a StartSynth multimode microwave instrument producing controlled irradiation at 2.45 GHz (Milestone S.r.l., Sorisole, Italy). The instrument is equipped with an industrial magnetron and a microwave diffuser located above the microwave chamber, with continuous microwave output power from 0 to 1400 W. Reaction times refer to hold times at the indicated temperatures, not to total irradiation times.

4.2. General procedure for the preparation of cycloadducts *4*

A mixture of *(E,E)*−3,5-bisarylidene-*N*-[(*S*)-(-)-methylbenzyl]−4-piperidones **1a–f** (1 mmol), isatin **2** (1 mmol), aminoester **3a-c** (1 mmol), and Et_3N (1 mmol) was heated in methanol at 100 °C for 10 mn under microwave irradiation (350 W). After completion of the reaction (TLC monitoring), the solvent was removed under vacuum. The crude residue was recrystallized in ethanol to give the enantiopure spirooxindolopyrrolidines **4**.

4.3. Crystal structure determination

Data collection was performed on a Bruker D8 Venture four-circle diffractometer from Bruker AXS GmbH (Billerica, Germany). CPAD detectors used were Photon II from Bruker AXS GmbH; X-ray sources: Microfocus source IμS; and microfocus source IμS Mo and Cu, respectively, from Incoatec GmbH with mirror opticsHELIOS and a single-hole collimator from Bruker AXS GmbH. Programs used for data collection were APEX4 Suite [84] (v2021.10–0) and integrated programs SAINT (V8.40A; integration) and SADABS (2018/7; absorption correction) from Bruker AXS GmbH [84]. The SHELX programs were used for further processing [85]. The solution of the crystal structure was done with the help of the program SHELXT [86], the structure refinement with SHELXL [87]. The processing and finalization of the crystal structure data was done with program OLEX2 v1.5 [88]. All non-hydrogen atoms were refined anisotropically. For the hydrogen atoms, the standard values of the SHELXL program were used with Uiso(H) = −1.2 Ueq (C) for CH_2 and CH and with Uiso(H) = −1.5 Ueq(C) for CH3. All H atoms were refined freely using independent values for each Uiso(H).

Crystal data for $C_{39}H_{37}N_3O_4$, M = 611.75 g•mol^{-1}, red-orange plates, crystal size 0.585 × 0.355 × 0.208 mm^3, monoclinic, space

Table 4
Toxicity risks, solubility, drug-likeness, and drug score of compounds 4c, 4k, 4j and 4l.

Entry	Toxicity risksa				Solubility	Drug likeness	Drug score
	Mutagenicity	Tumorigenicity	Irritancy	Reproductive effect			
4c	🟢	🟢	🟢	🔴	−6.09	4.06	0.15
4k	🟢	🟢	🟢	🟢	−6.31	4.07	0.15
4j	🟢	🟢	🟢	🟡	−7.06	4.26	0.13
4l	🟢	🟢	🟢	🟡	−7.72	2.18	0.12

Key: 🔴: High Risk 🟡: Medium Risk, 🟢: Low Risk.

group P21, $a = 12.7250(5)$ Å, $b = 13.50414(6)$ Å, $c = 19.8256(9)$ Å, $\alpha = 90°$, $\beta = 96.963(2)°$, $\gamma = 90°$; $V = 3265.98(2)$ Å3, $Z = 4$, Dcalc = 1.244 g/cm^3, $T = 100$ K, 2Θ range for data collection = 4.49 to 158.878°, R1 = 0.0308, wR2 = 0.0775 for 97,906 reflections with $I \geq 2\sigma$ (I) and 13,914 independent reflections. GOF = 1.034. Largest diff. peak/hole/e $Å-3$ 0.18/−0.19. Flack parameter 0.02(4). Data were collected using graphite monochromated CuK_α radiation $\lambda = 1.54178$ Å and have been deposited at the Cambridge Crystallographic Data Centre as CCDC 2,308,899. The data can be obtained free of charge from the Cambridge Crystallographic Data Centre via http://www.ccdc.cam.ac.uk/getstructures.

4.4. Molecular docking

4.4.1. Ligands and targets preparations

The 3D structures of four most active compounds: **4c, 4k, 4j** and **4l** were pre-optimized by means of the Molecular Mechanics using Force Field MM+. After that, all compounds were further optimized using the semi-empirical method AM1 [89], which is implemented in the Hyperchem 8.0.8 software [90].

The X-ray crystallographic structures of four different drug target proteins (Table S6) were downloaded from the RCSB Protein Databank (https://www.rcsb.org/), that is, multiple virulence factor regulator (MvfR) (PDB ID 4JVI) from *P. aeruginosa* [65], Topoisomerase IV (PDB ID 3FV5) from *E. coli* [91], RamR (PDB ID 6IE9) *S. enterica* [75], and heterologous protein expression (PDB ID 2RHL) from *B. subtilis* [92] were selected as antibacterial targets. Secreted aspartic protease (PDB ID 3Q70) from *C. albicans* [93] was selected as the antifungal target. The docking methodology is reported in our pervious study [31].

4.4.2. Drug-likeness prediction and ADME-Tox

TPSA, nROT, MW, LogP, Number of hydrogen bond acceptors (nHA) and Number of hydrogen bond donors (nHD) were calculated using the SwissADME server (http://www.swissadme.ch/, accessed on 20 October 2023) [94] in order to verify the different rules namely: Lipinski, Vaber, and Egan. In addition, we used pkCSM server (http://biosig.unimelb.edu.au/pkcsm/prediction, accessed on 20 October 2023) [95] in order to predict: the Absorption (Caco-2: Colon adenocarcinoma, HIA: Human intestinal absorption), Distribution (CNS: Central Nervous System permeability, BBB: Blood–Brain Barrier permeability), Metabolism (CYP1A2 inhibitor, CYP2C19 inhibitor,and CYP2D6 substrate), Excretion (Renal OCT2 substrate, and Total Clearance) and Toxicity (AMES toxicity, and hERG I and II Toxicity).

Funding

This research has been funded by Scientific Research Deanship at University of Ha'il - Saudi Arabia through project number RG-23 065.

CRediT authorship contribution statement

Hanen Jelizi: Resources. **Amani Toumi:** Methodology. **Faiza I.A. Abdella:** Project administration. **Ismail Daoud:** Validation. **Sarra Boudriga:** Writing – original draft, Formal analysis. **Asma K. Alshamari:** Software. **Tahani Y.A. Alanazi:** Formal analysis. **Ahlam Abdulrahman Alrashdi:** Conceptualization. **Hayet Edziri:** Visualization. **Michael Knorr:** Supervision, Writing – review & editing. **Jan-Lukas Kirchhoff:** Data curation. **Carsten Strohmann:** Investigation.

Declaration of competing interest

The authors declare no conflicts of interest.

Data availability

Data will be made available on request.

Acknowledgment

This research has been funded by Scientific Research Deanship at University of Ha'il - Saudi Arabia through project number RG-23 065.

Supplementary materials

The following supporting information can be found in the supplementary materials: compound characterization data of spirooxindoles **4a–l**, copies of NMR spectra of compounds **4a–l** (Figs. S1–S25), association of two independent molecules of **4g** (Fig. S26), fingerprint plots of 4 g (Fig. S27), and information related to the studied enzyme in the docking studies (Tables S1–S6).

Supplementary material associated with this article can be found, in the online version, at doi:10.1016/j.molstruc.2024.138104.

References

[1] M.A. Salam, M.Y. Al-Amin, M.T. Salam, J.S. Pawar, N. Akhter, A.A. Rabaan, M.A. A. Alqumber, Antimicrobial resistance: a growing serious threat for global public health, Healthcare 11 (2023) 1946, https://doi.org/10.3390/healthcare11131946.
[2] L. Serwecińska, Antimicrobials and antibiotic-resistant bacteria: a risk to the environment and to public health, Water 12 (2020) 3313, https://doi.org/10.3390/w12123313 (Basel).
[3] A. Talebi Bezmin Abadi, A.A. Rizvanov, T. Haertlé, N.L. Blatt, World health organization report: current crisis of antibiotic resistance, BioNanoSci 9 (2019) 778–788, https://doi.org/10.1007/s12668-019-00658-4.
[4] T.R. Walsh, A.C. Gales, R. Laxminarayan, P.C. Dodd, Antimicrobial resistance: addressing a global threat to humanity, PLoS Med. 20 (2023) e1004264, https://doi.org/10.1371/journal.pmed.1004264.
[5] S. Martínez-Álvarez, S. Sanz, C. Olarte, R. Hidalgo-Sanz, I. Carvalho, R. Fernández-Fernández, A. Campaña-Burguet, J. Latorre-Fernández, M. Zarazaga, C. Torres, Antimicrobial resistance in escherichia coli from the broiler farm environment, with detection of SHV-12-producing isolates, Antibiotics 11 (2022) 444, https://doi.org/10.3390/antibiotics11040444.
[6] D.G.J. Larsson, C.F. Flach, Antibiotic resistance in the environment, Nat. Rev. Microbiol. 20 (2022) 257–269, https://doi.org/10.1038/s41579-021-00649-x.
[7] S. Dhingra, N.A.A. Rahman, E. Peile, M. Rahman, M. Sartelli, M.A. Hassali, T. Islam, S. Islam, M. Haque, Microbial resistance movements: an overview of global public health threats posed by antimicrobial resistance, and how best to counter, Front. Public Health 8 (2020) 535668, https://doi.org/10.3389/fpubh.2020.535668.
[8] A. Amin, T. Qadir, P.K. Sharma, I. Jeelani, H. Abe, A Review on the medicinal and industrial applications of N-containing heterocycles, TOMCJ 16 (2022) e187410452209010, https://doi.org/10.2174/18741045-v16-e2209010.
[9] S. Majee, M.Sarav Shilpa, B.K. Banik, D. Ray, Recent advances in the green synthesis of active N-heterocycles and their biological activities, Pharmaceuticals 16 (2023) 873, https://doi.org/10.3390/ph16060873.
[10] S. Saleh Alghamdi, R. Saad Suliman, R. Awadh Alshehri, R. Suleiman Almahmoud, R. Ibrahim Alhujirey, N-Heterocycle derivatives: an update on the biological activity in correlation with computational predictions, J. Appl. Pharm. Sci. (2022), https://doi.org/10.7324/JAPS.2022.120504.
[11] D. Atukuri, R. Gunjal, N. Holagundi, B. Korlahalli, S. Gangannavar, K. Akkasali, Contribution of *N* -HETEROCYCLES towards anti-tubercular drug discovery (2014–2019); predicted and reengineered molecular frameworks, Drug Dev. Res 82 (2021) 767–783, https://doi.org/10.1002/ddr.21809.
[12] P. Bhutani, G. Joshi, N. Raja, N. Bachhav, P.K. Rajanna, H. Bhutani, A.T. Paul, R. Kumar, U.S. FDA approved drugs from 2015–June 2020: a perspective, J. Med. Chem. 64 (2021) 2339–2381, https://doi.org/10.1021/acs.jmedchem.0c01786.
[13] S. Kumari, K. Maddeboina, R.D. Bachu, S.H.S. Boddu, P.C. Trippier, A.K. Tiwari, Pivotal role of nitrogen heterocycles in Alzheimer's disease drug discovery, Drug Discov. Today 27 (2022) 103322, https://doi.org/10.1016/j.drudis.2022.07.007.
[14] D.K. Lang, R. Kaur, R. Arora, B. Saini, S. Arora, Nitrogen-containing heterocycles as anticancer agents: an overview, ACAMC 20 (2020) 2150–2168, https://doi.org/10.2174/1871520620666200705214917.
[15] A. Mermer, T. Keles, Y. Sirin, Recent studies of nitrogen containing heterocyclic compounds as novel antiviral agents: a review, Bioorg. Chem. 114 (2021) 105076, https://doi.org/10.1016/j.bioorg.2021.105076.
[16] L.M. Zhou, R.Y. Qu, G.F. Yang, An overview of spirooxindole as a promising scaffold for novel drug discovery, Expert Opin. Drug Discov. 15 (2020) 603–625, https://doi.org/10.1080/17460441.2020.1733526.
[17] B. Yu, Y.C. Zheng, X.J. Shi, P.P. Qi, H.M. Liu, Natural product-derived spirooxindole fragments serve as privileged substructures for discovery of new anticancer agents, Anti-Cancer Agents Med. Chem. Anti-Cancer Agents 16 (2016) 1315–1324.
[18] B. Yu, D.Q. Yu, H.M. Liu, Spirooxindoles: promising scaffolds for anticancer agents, Eur. J. Med. Chem. 97 (2015) 673–698, https://doi.org/10.1016/j.ejmech.2014.06.056.
[19] S.S. Panda, R.A. Jones, P. Bachawala, P.P. Mohapatra, Spirooxindoles as potential pharmacophores, Mini Rev. Med. Chem. 17 (2017) 1515–1536, https://doi.org/10.2174/1389557516666160624125108.

[20] N. Ye, H. Chen, E.A. Wold, P.Y. Shi, J. Zhou, Therapeutic potential of spirooxindoles as antiviral agents, ACS Infect. Dis 2 (2016) 382–392, https://doi.org/10.1021/acsinfecdis.6b00041.

[21] Y. Zheng, C.M. Tice, S.B. Singh, The use of spirocyclic scaffolds in drug discovery, Bioorg. Med. Chem. Lett. 24 (2014) 3673–3682, https://doi.org/10.1016/j.bmcl.2014.06.081.

[22] Molecular properties that influence the oral bioavailability of drug candidates, J. Med. Chem. (2023). https://pubs.acs.org/doi/10.1021/jm020017n. accessed September 14.

[23] B. Yu, Z. Yu, P.P. Qi, D.Q. Yu, H.M. Liu, Drug discovery using spirooxindole cores: success and Challenges [corrected], Eur. J. Med. Chem. 95 (2015) 35–40, https://doi.org/10.1016/j.ejmech.2015.03.020.

[24] M.J. Buskes, A. Coffin, D.M. Troast, R. Stein, M.J. Blanco, Accelerating drug discovery: synthesis of complex chemotypes via multicomponent reactions, ACS Med. Chem. Lett. 14 (2023) 376–385, https://doi.org/10.1021/acsmedchemlett.3c00012.

[25] Q. Yu, P. Guo, J. Jian, Y. Chen, J. Xu, Nine-step total synthesis of (−)-strychnofoline, Chem. Commun. 54 (2018) 1125–1128, https://doi.org/10.1039/C7CC08938D.

[26] S. Mignani, S. El Kazzouli, M.M. Bousmina, J.P. Majoral, Dendrimer space exploration: an assessment of dendrimers/dendritic scaffolding as inhibitors of protein–protein interactions, a potential new area of pharmaceutical development, Chem. Rev. 114 (2014) 1327–1342, https://doi.org/10.1021/cr400362r.

[27] A.K. Gupta, M. Bharadwaj, A. Kumar, R. Mehrotra, Spiro-oxindoles as a promising class of small molecule inhibitors of p53–MDM2 interaction useful in targeted cancer therapy, Top Curr. Chem. (Z) 375 (2016) 3, https://doi.org/10.1007/s41061-016-0089-0.

[28] H. Shi, J. Jiang, H. Zhang, H. Jiang, Z. Su, D. Liu, L. Jie, F. He, Antibacterial spirooxindole alkaloids from Penicillium brefeldianum inhibit dimorphism of pathogenic smut fungi, Front. Microbiol. 13 (2022). https://www.frontiersin.org/articles/10.3389/fmicb.2022.1046099. accessed September 14, 2023.

[29] M. Gul, E. Turk Celikoglu, O. Idil, G. Tas, E. Pelit, Synthesis, antimicrobial activity and molecular docking studies of spiroquinoline-indoline-dione and spiropyrazolo-indoline-dione derivatives, Sci. Rep. 13 (2023) 1676, https://doi.org/10.1038/s41598-023-27777-z.

[30] N. Chouchène, A. Toumi, S. Boudriga, H. Edziri, M. Sobeh, M.A.O. Abdelfattah, M. Askri, M. Knorr, C. Strohmann, L. Brieger, A. Soldera, Antimicrobial activity and DFT studies of a novel set of spiropyrrolidines tethered with thiochroman-4-one/Chroman-4-one Scaffolds, Molecules 27 (2022) 582, https://doi.org/10.3390/molecules27030582.

[31] A. Toumi, F.I.A. Abdella, S. Boudriga, T.Y.A. Alanazi, A.K. Alshamari, A. A. Alrashdi, A. Dbeibia, K. Hamden, I. Daoud, M. Knorr, J.L. Kirchhoff, C. Strohmann, Synthesis of tetracyclic spirooxindolepyrrolidine-engrafted hydantoin scaffolds: crystallographic analysis, molecular docking studies and evaluation of their antimicrobial, anti-inflammatory and analgesic activities, Molecules 28 (2023) 7443, https://doi.org/10.3390/molecules28217443.

[32] S. Boudriga, S. Haddad, V. Murugaiyah, M. Askri, M. Knorr, C. Strohmann, C. Golz, Three-component access to functionalized spiropyrrolidine heterocyclic scaffolds and their cholinesterase inhibitory activity, Molecules 25 (2020) 1963, https://doi.org/10.3390/molecules25081963.

[33] A. Toumi, S. Boudriga, K. Hamden, M. Sobeh, M. Cheurfa, M. Askri, M. Knorr, C. Strohmann, L. Brieger, Synthesis, antidiabetic activity and molecular docking study of rhodanine-substitued spirooxindole pyrrolidine derivatives as novel α-amylase inhibitors, Bioorg. Chem. 106 (2021) 104507, https://doi.org/10.1016/j.bioorg.2020.104507.

[34] N. Nivetha, R.Mary Martiz, S.M. Patil, R. Ramu, S. Sreenivasa, S. Velmathi, Benzodioxole grafted spirooxindole pyrrolidinyl derivatives: synthesis, characterization, molecular docking and anti-diabetic activity, RSC Adv. 12 (2022) 24192–24207, https://doi.org/10.1039/D2RA04452H.

[35] C. Teja, S.N. Babu, A. Noor, J.A. Daniel, S.A. Devi, F.R. Nawaz Khan, Cu/TEMPO catalyzed dehydrogenative 1,3-dipolar cycloaddition in the synthesis of spirooxindoles as potential antidiabetic agents, RSC Adv. 10 (2020) 12262–12271, https://doi.org/10.1039/D0RA01553A.

[36] S. Haddad, S. Boudriga, T.N. Akhaja, J.P. Raval, F. Porzio, A. Soldera, M. Askri, M. Knorr, Y. Rousselin, M.M. Kubicki, D. Rajani, A strategic approach to the synthesis of functionalized spirooxindole pyrrolidine derivatives: *in vitro* antibacterial, antifungal, antimalarial and antitubercular studies, New J. Chem. 39 (2015) 520–528, https://doi.org/10.1039/C4NJ01008F.

[37] B.S. Allaka, S. Basavoju, E. Madhu Rekha, D. Sriram, G.Rama Krishna, Design and synthesis of novel quinazolinyl-bisspirooxindoles as potent anti-tubercular agents: an ultrasound-promoted methodology, Mol. Divers. 27 (2023) 1427–1436, https://doi.org/10.1007/s11030-022-10500-x.

[38] V. Pogaku, V.S. Krishna, C. Balachandran, K. Rangan, D. Sriram, S. Aoki, S. Basavoju, The design and green synthesis of novel benzotriazoloquinolinyl spirooxindolopyrrolizidines: antimycobacterial and antiproliferative studies, New J. Chem. 43 (2019) 17511–17520, https://doi.org/10.1039/C9NJ03802G.

[39] G. Meera, K.R. Rohit, S. Saranya, G. Anilkumar, Microwave assisted synthesis of five membered nitrogen heterocycles, RSC Adv. 10 (2020) 36031–36041, https://doi.org/10.1039/D0RA05150K.

[40] S. Gulati, S.E. John, N. Shankaraiah, Microwave-assisted multicomponent reactions in heterocyclic chemistry and mechanistic aspects, Beilstein J. Org. Chem. 17 (2021) 819–865, https://doi.org/10.3762/bjoc.17.71.

[41] P. Khanna, L. Khanna, S.J. Thomas, A.M. Asiri, S.S. Panda, Microwave assisted synthesis of spiro heterocyclic systems: a review, COC 22 (2018) 67–84, https://doi.org/10.2174/1385272821666170818161517.

[42] D.B. Upadhyay, R.M. Vala, S.G. Patel, P.J. Patel, C. Chi, H.M. Patel, Water mediated TBAB catalyzed synthesis of spiro-indoline-pyrano[3,2-c]quinolines as α-amylase inhibitor and in silico studies, J. Mol. Struct. 1273 (2023) 134305, https://doi.org/10.1016/j.molstruc.2022.134305.

[43] S.G. Patel, R.M. Vala, P.J. Patel, D.B. Upadhyay, V. Ramkumar, R.L. Gardas, H. M. Patel, Synthesis, crystal structure and *in silico* studies of novel 2,4-dimethoxy-tetrahydropyrimido[4,5- *b*]quinolin-6(7 *H*)-ones, RSC Adv. 12 (2022) 18806–18820, https://doi.org/10.1039/D2RA02694E.

[44] D.M. Patel, P.J. Patel, H.M. Patel, Catalytic stereoselective multicomponent reactions for the synthesis of spiro derivatives: recent progress, Eur. J. Org. Chem. 2022 (2022) e202201119, https://doi.org/10.1002/ejoc.202201119.

[45] M. Krátký, K. Nováčková, K. Svrčková, M. Švarcová, Š. Štěpánková, New 3-amino-2-thioxothiazolidin-4-one-based inhibitors of acetyl- and butyryl-cholinesterase: synthesis and activity, Future Med. Chem. 16 (2024) 59–74, https://doi.org/10.4155/fmc-2023-0268.

[46] E.M.M. Abdelraheem, S. Shaabani, A. Dömling, Macrocycles: MCR synthesis and applications in drug discovery, Drug Discovery Today Technol. 29 (2018) 11–17, https://doi.org/10.1016/j.ddtec.2018.06.008.

[47] R. Sunke, P.V. Babu, S. Yellanki, R. Medishetti, P. Kulkarni, M. Pal, Ligand-free MCR for linking quinoxaline framework with a benzimidazole nucleus: a new strategy for the identification of novel hybrid molecules as potential inducers of apoptosis, Org. Biomol. Chem. 12 (2014) 6800, https://doi.org/10.1039/C4OB01268B.

[48] T. Zarganes-Tzitzikas, A. Dömling, Modern multicomponent reactions for better drug syntheses, Org. Chem. Front. 1 (2014) 834–837, https://doi.org/10.1039/C4QO00088A.

[49] R.C. Cioc, E. Ruijter, R.V.A. Orru, Multicomponent reactions: advanced tools for sustainable organic synthesis, Green Chem. 16 (2014) 2958–2975, https://doi.org/10.1039/C4GC00013G.

[50] G.A. Coppola, S. Pillitteri, E.V. Van Der Eycken, S.L. You, U.K. Sharma, Multicomponent reactions and photo/electrochemistry join forces: atom economy meets energy efficiency, Chem. Soc. Rev. 51 (2022) 2313–2382, https://doi.org/10.1039/D1CS00510C.

[51] E. Ruijter, R. Scheffelaar, R.V.A. Orru, Multicomponent reaction design in the quest for molecular complexity and diversity, Angew. Chem. Int. Ed. 50 (2011) 6234–6246, https://doi.org/10.1002/anie.201006515.

[52] M. Hossain, S. Das, U. Das, A. Doroudi, J. Zhu, J.R. Dimmock, Novel hybrid molecules of 3,5-bis(benzylidene)-4-piperidones and dichloroacetic acid which demonstrate potent tumour-selective cytotoxicity, Bioorg. Med. Chem. Lett. 30 (2020) 126878, https://doi.org/10.1016/j.bmcl.2019.126878.

[53] A. Basiri, B.M. Abd Razik, M.O. Ezzat, Y. Kia, R.S. Kumar, A.I. Almansour, N. Arumugam, V. Murugaiyah, Synthesis and cholinesterase inhibitory activity study of new piperidone grafted spiropyrrolidines, Bioorg. Chem. 75 (2017) 210–216, https://doi.org/10.1016/j.bioorg.2017.09.019.

[54] M. Zuo, X. Xu, Z. Xie, R. Ge, Z. Zhang, Z. Li, J. Bian, Design and synthesis of indoline thiohydantoin derivatives based on enzalutamide as antiproliferative agents against prostate cancer, Eur. J. Med. Chem. 125 (2017) 1002–1022, https://doi.org/10.1016/j.ejmech.2016.10.049.

[55] S. Lawson, N. Arumugam, A.I. Almansour, R. Suresh Kumar, S. Thangamani, Dispiropyrrolidine tethered piperidone heterocyclic hybrids with broad-spectrum antifungal activity against Candida albicans and Cryptococcus neoformans, Bioorg. Chem. 100 (2020) 103865, https://doi.org/10.1016/j.bioorg.2020.103865.

[56] A. Toumi, S. Boudriga, Y.M. Mandour, A.A. Mekki, M. Knorr, C. Strohmann, J. L. Kirchhoff, M. Sobeh, Design of novel enantiopure dispirooxindolopyrrolidine-piperidones as promising candidates toward COVID-19: asymmetric synthesis, crystal structure and in silico studies, Molecules 27 (2022) 3945, https://doi.org/10.3390/molecules27123945.

[57] S. Haddad, S. Boudriga, F. Porzio, A. Soldera, M. Askri, D. Sriram, P. Yogeeswari, M. Knorr, Y. Rousselin, M.M. Kubicki, Synthesis of novel dispiropyrrolothiazoles by three-component 1,3-dipolar cycloaddition and evaluation of their antimycobacterial activity, RSC Adv. 4 (2014) 59462–59471, https://doi.org/10.1039/C4RA11940A.

[58] A. Toumi, S. Boudriga, K. Hamden, I. Daoud, M. Askri, A. Soldera, J.F. Lohier, C. Strohmann, L. Brieger, M. Knorr, Diversity-oriented synthesis of spiropyrrolo [1,2- *a*]isoquinoline derivatives via diastereoselective and regiodivergent three-component 1,3-dipolar cycloaddition reactions: *in vitro* and *in vivo* evaluation of the antidiabetic activity of rhodanine analogues, J. Org. Chem. 86 (2021) 13420–13445, https://doi.org/10.1021/acs.joc.1c01544.

[59] M.B. Hammouda, S. Boudriga, K. Hamden, M. Askri, M. Knorr, C. Strohmann, L. Brieger, A. Krupp, E.H. Anouar, M. Snoussi, K. Aouadi, A. Kadri, New spiropyrrolothiazole derivatives bearing an oxazolone moiety as potential antidiabetic agent: design, synthesis, crystal structure, Hirshfeld surface analysis, ADME and molecular docking studies, J. Mol. Struct. 1254 (2022) 132398, https://doi.org/10.1016/j.molstruc.2022.132398.

[60] S. Balani, G. Miwa, L.S. Gan, J.T. Wu, F. Lee, Strategy of utilizing in vitro and in vivo ADME tools for lead optimization and drug candidate selection, CTMC 5 (2005) 1033–1038, https://doi.org/10.2174/156802605774297038.

[61] H.D. Flack, On enantiomorph-polarity estimation, Acta Crystallogr. A Found. Crystallogr. 39 (1983) 876–881, https://doi.org/10.1107/S0108767383001762.

[62] M.A. Spackman, D. Jayatilaka, Hirshfeld surface analysis, CrystEngComm 11 (2009) 19–32, https://doi.org/10.1039/B818330A.

[63] P.R. Spackman, M.J. Turner, J.J. McKinnon, S.K. Wolff, D.J. Grimwood, D. Jayatilaka, M.A. Spackman, *CrystalExplorer* : a program for Hirshfeld surface analysis, visualization and quantitative analysis of molecular crystals, J. Appl. Crystallogr. 54 (2021) 1006–1011, https://doi.org/10.1107/S1600576721002910.

[64] Rattan, A. Antimicrobials in Laboratory Medicine; B.I. Churchill Livingstone: new Delhi, India, 2000; Volume 85, p. 108., in: n.d.
[65] A. Ilangovan, M. Fletcher, G. Rampioni, C. Pustelny, K. Rumbaugh, S. Heeb, M. Cámara, A. Truman, S.R. Chhabra, J. Emsley, P. Williams, Structural basis for native agonist and synthetic inhibitor recognition by the pseudomonas aeruginosa quorum sensing regulator PqsR (MvfR), PLoS Pathog. 9 (2013) e1003508, https://doi.org/10.1371/journal.ppat.1003508.
[66] R.P.D. Bank, RCSB PDB - 3FV5: crystal Structure of E. coli Topoisomerase IV co-complexed with inhibitor, (n.d.). https://www.rcsb.org/structure/3fv5 (accessed November 29, 2023).
[67] S. Yamasaki, R. Nakashima, K. Sakurai, S. Baucheron, E. Giraud, B. Doublet, A. Cloeckaert, K. Nishino, Crystal structure of the multidrug resistance regulator RamR complexed with bile acids, Sci. Rep. 9 (2019) 177, https://doi.org/10.1038/s41598-018-36025-8.
[68] A. Raymond, S. Lovell, D. Lorimer, J. Walchli, M. Mixon, E. Wallace, K. Thompkins, K. Archer, A. Burgin, L. Stewart, Combined protein construct and synthetic gene engineering for heterologous protein expression and crystallization using Gene Composer, BMC Biotechnol. 9 (2009) 37, https://doi.org/10.1186/1472-6750-9-37.
[69] Koester, H.,Heine, A.,Klebe, G. The bindingmode of HIV-1 protease inhibitors to pepsin-like aspartic proteinases To be Published, in: 2024.
[70] Molecular modelling of protein-carbohydrate interactions. Docking of monosaccharides in the binding site of concanavalin A | Glycobiology | Oxford Academic, (n.d.). https://academic.oup.com/glycob/article-abstract/1/6/631/560688 (accessed November 29, 2023).
[71] R.C. Wade, P.J. Goodford, The role of hydrogen-bonds in drug binding, Prog. Clin. Biol. Res. 289 (1989) 433–444.
[72] Synthesis, in-vitro and in-silico antibacterial and computational studies of selected thiosemicarbazone-benzaldehyde derivatives as potential antibiotics | SN Applied Sciences, (n.d.). https://link.springer.com/article/10.1007/s42452-023-05429-1 (accessed November 29, 2023).
[73] Virtual screening of some heterocyclic structures toward novel antibacterial agents | SpringerLink, (n.d.). https://link.springer.com/article/10.1007/s13738-017-1262-2 (accessed November 29, 2023).
[74] M. Aarjane, S. Slassi, B. Tazi, A. Amine, Synthesis and biological evaluation of novel isoxazole derivatives from acridone, Arch. Pharm. 354 (2021) 2000261, https://doi.org/10.1002/ardp.202000261 (Weinheim).
[75] S. Yamasaki, R. Nakashima, K. Sakurai, S. Baucheron, E. Giraud, B. Doublet, A. Cloeckaert, K. Nishino, Crystal structure of the multidrug resistance regulator RamR complexed with bile acids, Sci. Rep. 9 (2019) 177, https://doi.org/10.1038/s41598-018-36025-8.
[76] J. Mehta, R. Rolta, K. Dev, Role of medicinal plants from North Western Himalayas as an efflux pump inhibitor against MDR AcrAB-TolC Salmonella enterica serovar typhimurium: *in vitro* and In silico studies, J. Ethnopharmacol. 282 (2022) 114589, https://doi.org/10.1016/j.jep.2021.114589.
[77] T. Alorini, I. Daoud, A.N. Al-Hakimi, F. Alminderej, A.E.A.E. Albadri, An experimental and theoretical investigation of antimicrobial and anticancer properties of some new Schiff base complexes, Res. Chem. Intermed. 49 (2023) 1701–1730, https://doi.org/10.1007/s11164-022-04922-3.
[78] A. Miguel, J. Hsin, T. Liu, G. Tang, R.B. Altman, K.C. Huang, Variations in the Binding Pocket of an Inhibitor of the Bacterial Division Protein FtsZ across Genotypes and Species, PLoS Comput. Biol. 11 (2015) e1004117, https://doi.org/10.1371/journal.pcbi.1004117.
[79] Z. Kibou, N. Aissaoui, I. Daoud, J.A. Seijas, M.P. Vázquez-Tato, N. Klouche Khelil, N. Choukchou-Braham, Efficient synthesis of 2-aminopyridine derivatives: antibacterial activity assessment and molecular docking studies, Molecules 27 (2022) 3439, https://doi.org/10.3390/molecules27113439.
[80] B.O. Aljohny, A. Rauf, Y. Anwar, S. Naz, A. Wadood, Antibacterial, antifungal, antioxidant, and docking studies of potential dinaphthodiospyrols from *Diospyros lotus* Linn roots, ACS Omega 6 (2021) 5878–5885, https://doi.org/10.1021/acsomega.0c06297.
[81] https://en.wikipedia.org/wiki/Lipinski%27s_rule_of_five, (2024).
[82] (https://www.solvobiotech.com/transporters/oct2), (2024).
[83] Organic Chemistry Portal.; 2022. Available at: https://www.organic-chemistry.org/prog/peo/(Accessed on 10 November 2023)., (n.d.).
[84] Bruker, Apex 4, Bruker AXS Inc., 2021.
[85] G.M. Sheldrick, A short history of SHELX, Acta Cryst. A 64 (2008) 112–122, https://doi.org/10.1107/S0108767307043930.
[86] G.M. Sheldrick, SHELXT – Integrated space-group and crystal-structure determination, Acta Cryst. A 71 (2015) 3–8, https://doi.org/10.1107/S2053273314026370.
[87] G.M. Sheldrick, Crystal structure refinement with SHELXL, Acta Cryst. C 71 (2015) 3–8, https://doi.org/10.1107/S2053229614024218.
[88] O.V. Dolomanov, L.J. Bourhis, R.J. Gildea, J.a.K. Howard, H. Puschmann, OLEX2: a complete structure solution, refinement and analysis program, J. Appl. Cryst. 42 (2009) 339–341, https://doi.org/10.1107/S0021889808042726.
[89] Optimization of parameters for semiempirical methods V: modification of NDDO approximations and application to 70 elements | Journal of Molecular Modeling, (n.d.). https://link.springer.com/article/10.1007/s00894-007-0233-4 (accessed August 30, 2023).
[90] HyperChem v8. Molecular Modelling System, Hypercube Inc., 1115 NW 4th Street, Gainesville, FL 32601, USA (2009), (n.d.).
[91] R.P.D. Bank, RCSB PDB - 3FV5: Crystal Structure of E. Coli Topoisomerase IV co-Complexed With inhibitor, (n.d.). https://www.rcsb.org/structure/3fv5 (accessed January 24, 2024).
[92] A. Raymond, S. Lovell, D. Lorimer, J. Walchli, M. Mixon, E. Wallace, K. Thompkins, K. Archer, A. Burgin, L. Stewart, Combined protein construct and synthetic gene engineering for heterologous protein expression and crystallization using Gene Composer, BMC Biotechnol. 9 (2009) 37, https://doi.org/10.1186/1472-6750-9-37.
[93] Search by PDB author - Protein Data Bank Japan, (n.d.). https://pdbj.org/search/pdb-author?query=%22Koester%2C+H.%22 (accessed January 24, 2024).
[94] A. Daina, O. Michielin, V. Zoete, SwissADME: a free web tool to evaluate pharmacokinetics, drug-likeness and medicinal chemistry friendliness of small molecules, Sci. Rep. 7 (2017) 42717, https://doi.org/10.1038/srep42717.
[95] D.E.V. Pires, T.L. Blundell, D.B. Ascher, pkCSM: predicting small-molecule pharmacokinetic and toxicity properties using graph-based signatures, J. Med. Chem. 58 (2015) 4066–4072, https://doi.org/10.1021/acs.jmedchem.5b00104.